RESEARCH ARTICLE

Basin Research   IAS EAGE WILEY

Lithological influence on sill geometry in sedimentary basins: Controls and recognition in reflection seismic data

Martin Kjenes[1] | **Christian Haug Eide[1]** | **Agustin Argüello Scotti[1]** | **Isabelle Lecomte[1]** | **Nick Schofield[2]** | **Anna Bøgh[3]**

[1]Department of Earth Science, University of Bergen, Bergen, Norway

[2]Geology and Petroleum Geology, School of Geosciences, University of Aberdeen, Aberdeen, UK

[3]DMR Miljø og Geoteknik AS, Copenhagen, Denmark

Correspondence
Martin Kjenes, Department of Earth Science, University of Bergen, Allégaten 41, 5007 Bergen, Norway.
Email: martinkjenes@gmail.com

Funding information
Universitetet i Bergen

Abstract

Sills play a leading role in the transport of magma in sedimentary basins. The contact between sills and host rocks reflects the acting emplacement processes during sill propagation and evolution. Recent studies have shown that the propagation of sills and dykes is strongly influenced by the lithology of the host rocks, but none have detailed documentation of marginal features in large-scale intrusive complexes. Three-dimensional seismic data is the primary method of mapping and investigating such complexes, but it is difficult to accurately image sills due to their low thickness compared to seismic resolution. By understanding the relationship between local lithology and marginal sill features, we can better understand the imaging of sills in seismic datasets and their resulting geometry. In this study, we present a seismic-scale sill analogue through multiple high-resolution three-dimensional models, with corresponding logs and field observations from Cedar Mountains, San Rafael Swell, US. This model was further used to develop a synthetic seismic dataset, providing us with a strong control on which marginal sill features fall beneath seismic resolution. We found that lithology plays a critical control in sill geometry and morphology. In Cedar Mountains, sills emplaced within massive sandstones frequently exhibit strata-discordant base contact with the host rock. Conversely, sills found within heterolithic intervals and mudstones typically display strata-concordant base contact with the host rocks. Sills within heterolithic intervals also tend to exhibit a more complex segmentation with multiple broken bridges. Furthermore, our findings show that sills are more than 3.7 times more likely to intrude in mudstone compared to sandstone and heterolithic intervals. These results suggest how sill geometries can be adapted to interpret lithology in seismic datasets from sedimentary basins with little to no well control. We anticipate that our findings may provide better knowledge for interpreting sills in sedimentary basins and contribute to developing more sophisticated geomechanical emplacement models for igneous intrusions.

KEYWORDS
Entrada Formation, field analogues, sedimentary basins, sill emplacement, synthetic seismic

1 | INTRODUCTION

Sills and dykes represent key components of *volcanic plumbing systems* (e.g. Jerram & Bryan, 2018). While dykes have traditionally been considered as the dominant storage for magma in the subsurface, seismic reflection studies have shown that sill complexes not only act as a major part of the plumbing system but perhaps a leading role in the transport of magma in sedimentary basins (Cartwright & Møller Hansen, 2006; Eide et al., 2022; Magee et al., 2016; Yao & Mungall, 2022). In the last 20 years, three-dimensional seismic reflection data have been used extensively to map and characterize large-scale intrusive complexes within the subsurface, but various problems are related to the seismic imaging of igneous intrusions (e.g. Planke et al., 2018; Rabbel et al., 2018; Senger et al., 2017). Sills often represent thin geological layers of elevated acoustic impedance (p-wave velocity multiplied with density) compared to host rocks, and recent studies have shown that many sills are too thin to be recognized in seismic datasets and locally up to 88% of sills can be missing when interpreting seismic data in volcanic basins (Schofield et al., 2015). Studies of sills and their respective constraints regarding emplacement have also been conducted on smaller scales, such as numerical modelling (e.g. Haug et al., 2017), laboratory experiments (e.g. Kavanagh et al., 2017), field studies (e.g. Spacapan et al., 2017) and remote sensing (e.g. Richardson et al., 2015). Despite the large number of studies on sill emplacement, only a few studies have been directed to the lithological influence of sill emplacement and its importance for sill geometry. Understanding how sedimentary heterogeneity influences sill development on larger scales (tens meters to kilometres) may support current forecasting of volcanic eruptions, utilization of subsurface resources and improvement of general basin understanding.

This study investigates how sedimentary and lithologic heterogeneity influence sill propagation and -evolution of sill intrusions. Our dataset consists of large three-dimensional models with corresponding logs gathered from the Cedar Mountains, a 3.5 km long cliff-face in the San Rafael Volcanic Field (Utah, USA) (Figure 1) showing sills with varying sill architecture and different morphologies. This high-resolution dataset has further been used for synthetic seismic modelling to investigate what geometries are lacking in seismic datasets compared to field analogues. With a high resolution of 0.84–1.50 cm/pixel, these models provide an excellent opportunity to examine the sills on multiple kilometres to a few centimetres. Specifically, the goals of this study are three-fold: to (1) document differing contact morphologies between sills and various sedimentary host rocks; (2) investigate how host rock heterogeneity may influence emplacement mechanisms of sills; and (3) explore how sill geometries could be influenced by lithologies in subsurface sedimentary basins. The cliffs in the San Rafael Volcanic Field were chosen due to the well-preserved contacts between sills and sedimentary host rock and the exceptional scale of the outcrops. We see the sill architecture and geometry change significantly at various scales (e.g. 1 m–1 km). A key question is how host rock heterogeneity influences the large-scale architecture of sills, and how the overall emplacement changes during propagation through different sedimentary intervals.

2 | EMPLACEMENT MECHANISMS OF SILLS

2.1 | Host rock properties

Igneous sheet intrusions have traditionally been thought of as magma-driven fractures, in which the emplacement mechanisms are still uncertain (Airoldi et al., 2011). However, recent studies have shown that various factors of host rock properties, such as lithology (e.g. Schofield et al., 2012), degree of compaction (e.g. Schofield et al., 2010), cohesion (e.g. Schmiedel et al., 2017; Schofield, Brown, et al., 2012), elastic moduli and shear moduli (e.g. Haug et al., 2017, 2018), play a significant role in their emplacement. Additionally, factors such as magma viscosity (e.g. Burchardt et al., 2019), magma driving pressure relative to tectonic stress (e.g. Gill & Walker, 2020), depth of emplacement (e.g. Eide et al., 2022; Gill & Walker, 2020; Schofield, Brown, et al., 2012) and remote stress state (e.g. Rubin, 1993) can also affect intrusion morphology.

The importance of host rock lithology has received increased attention in recent years (e.g. Eide et al., 2017; Kavanagh et al., 2006; Magee et al., 2012). Studies carried out by Schofield et al. (2012) suggest that lithology can be broadly categorized into two types: brittle and non-brittle or ductile conditions. Brittle conditions refer to well-consolidated and mechanically strong host rocks (Figure 2a), while non-brittle represents poorly consolidated, mechanically weak, and heterogeneous host rocks (Figure 2b). Traditionally, sills emplaced within brittle fracture-driven conditions often show steps and bridges, which are structures that form when different sill segments either underlap or overlap, respectively (e.g. Schofield et al., 2012). As two overlapping sills inflate, a series of open tensile fractures will open perpendicular to the bridge axis in the zones of maximum flexure (Schofield et al., 2012). These fractures may further grow and unite the two overlapping sill segments, causing the two sills to coalesce into a connected system of sills (Schofield et al., 2012). Such emplacement structures have also been observed in non-brittle conditions (e.g. Galland et al., 2019).

FIGURE 1 Map overview of the Cedar Mountains. Showing locations of the different models (black lines), other local sills (green lines), bridge-propagation directions (yellow arrows), dykes (red lines) and conduits (red dots).
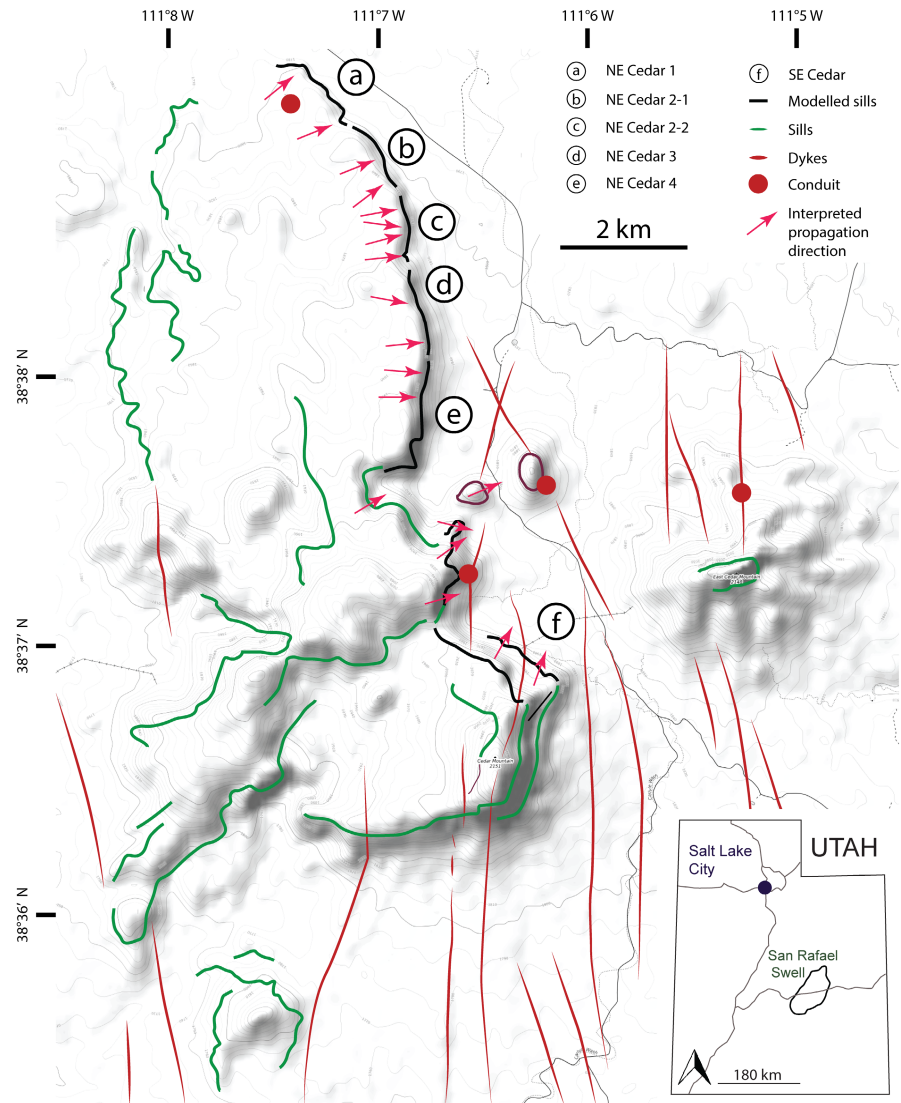
Non-brittle conditions are split down to host rocks with low cohesiveness and mechanical strenght, such as uncemented sediments, which will often exhibit ductile behaviour during magma emplacement. Non-brittle conditions are split down into two subsets: (i) primary non-brittle behaviour, inherently weak host rocks, and (ii) triggered non-brittle behaviour, were processes such as fluidization or direct heating, e.g. coal). Fluidization is a result of dynamic interaction between magma and sediments and forms a zone of incoherent, ragged, or clast-like mixture of host rock sediment and igneous rock known as '*peperite*' (Duffield et al., 1986; Skilling et al., 2002). Such zones are often, if not exclusively, related to boiling of pore-fluid or volatiles.

2.2 | Propagation models

The elastic-brittle propagation models are considered the most traditional emplacement model for sheet intrusions

and split into the following: (1) the *tensile elastic fracture-splitting model* (Figure 2c) and (2) the *Barenblatt-cohesive zone model* (Figure 2d). The first model conforms to linear elastic fracture mechanics and involves fractures with slit-like geometry and wedge-shaped (tapered) tips (Pollard, 1973). This model shows that the intrusion tip propagates by the tensile opening of the host rock (Pollard, 1973; Spacapan et al., 2017), in which the opening vector is dominantly perpendicular to the contacts. Thus, Pollard (1973) inferred the presence of a tip cavity, between the magma front and the intrusion tip, which is filled with exsolved volatiles from either magma or host rock. In this model, the host rock bends to accommodate the intrusion thickness (e.g. Stephens et al., 2021). The second model, the *Barenblatt-cohesive zone model*, is an extension of the tensile elastic fracture-splitting model (Rubin, 1993) but includes a cohesive process zone at the front of the fracture. The cohesive stresses in this zone act to resist dilation and are on the order of rock tensile strength (e.g. Rubin, 1993). This model typically involves
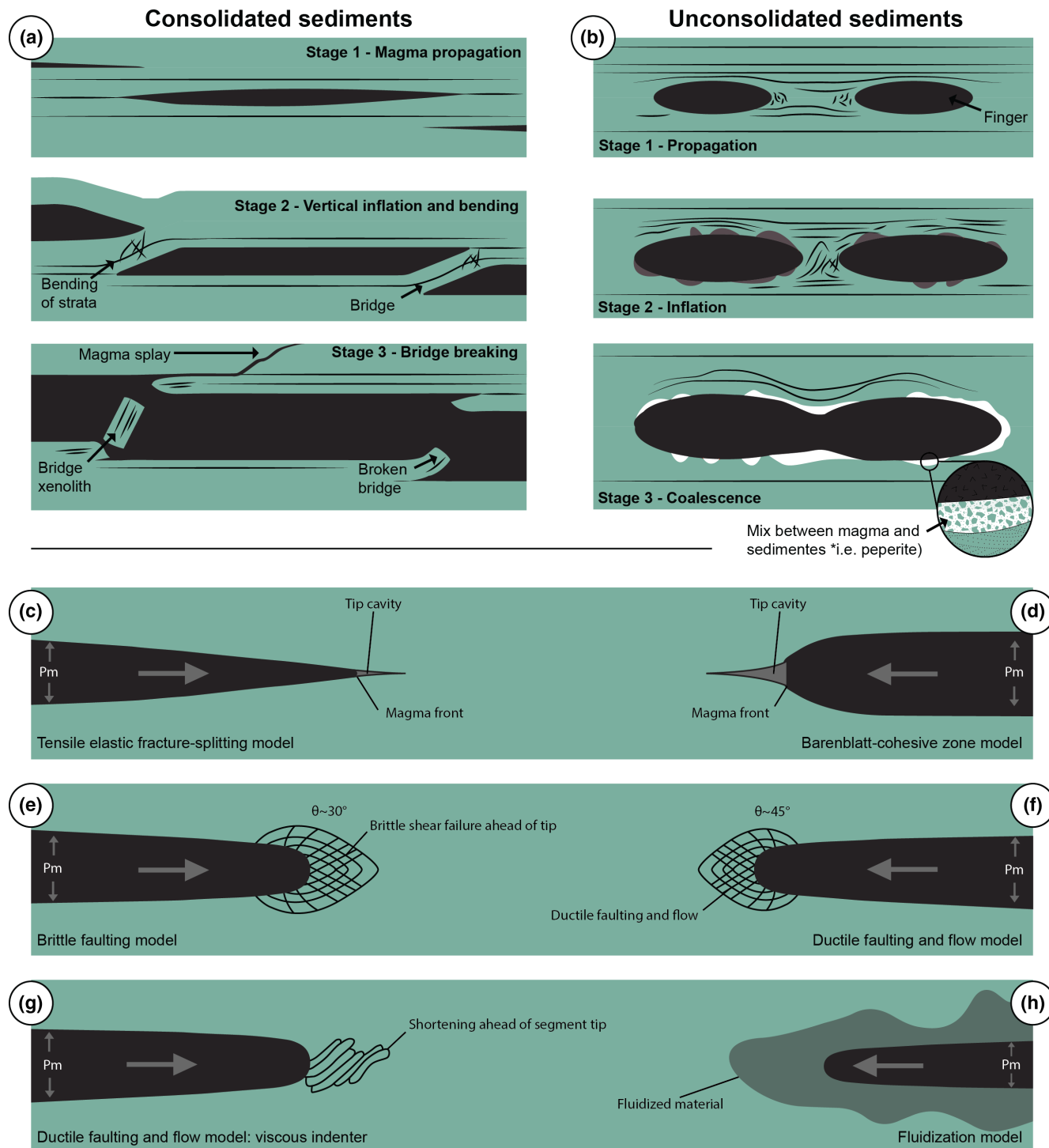
FIGURE 2 Overview of sill emplacement structures and propagation models in consolidated (a) and unconsolidated (b) host rocks. Modified after Schofield, Brown, et al. (2012) and Stephens et al. (2021). (a) Development and relationship of broken bridges. (b) Evolutionary stages of magma fingers. (c) Elastic-splitting model. (d) Barenblatt-cohesive model. (e) Brittle faulting model. (f) Ductile faulting and flow model. (g) Viscous indenter model. (h) Fluidization model.

blunting of intrusion tips if the magma driving pressure is insufficient to support further propagation of the fracture plane, due to inflation and rounding of the magma front (e.g. Stephens et al., 2021).

Non-brittle models, however, include multiple propagation models such as (1) *brittle faulting model* (Figure 2e)

(e.g. Pollard, 1973), (2) *ductile faulting and flow model* (Figure 2f,g) (e.g. Pollard, 1973), and (3) *fluidization model* (Figure 2h) (e.g. Schofield et al., 2012). These models infer that the host rock behaves as a sheared or viscous medium ahead of the propagating tip (Schofield et al., 2012; Spacapan et al., 2017). The faulting models (brittle, ductile

and flow) suggest shearing, buckling, folding faulting and/or ductile flow of the host rock in front of the intrusion tip due to sill propagation (Pollard, 1973; Spacapan et al., 2017). This deformation results in a thickening of the host rock ahead of a rounded or blunt intrusion tip, of a magnitude similar to the thickness of the intrusion (e.g. Pollard, 1973; Spacapan et al., 2017). Multiple studies have shown that magma viscosity plays a major mechanical role during the emplacement of sills (Bunger & Cruden, 2011; Galland et al., 2014; Michaut, 2011) and that rock formations can be complex brittle or ductile mechanical systems (Spacapan et al., 2017). This natural complexity is accounted for in the conceptual viscous indenter model (Figure 2g) (Abdelmalak et al., 2012; Donnadieu & Merle, 1998; Mathieu et al., 2008; Spacapan et al., 2017). *The fluidization model* (Figure 2h) is generally associated with the local heating of pore-fluids or organic matter close to the intrusion. The heat diffuses in the host rock, which leads to increasing fluid pressure until it exceeds the host rock cohesion. Thus, causing disaggregation, flow and/or incoherent disruption of the host rock (Kokelaar, 1982; Schofield et al., 2010, 2012). The *fluidization model* is often associated with intrusion emplaced within unconsolidated, or poorly consolidated, sedimentary material with low or zero cohesion (Kokelaar, 1982; Schofield et al., 2010, 2012).

3 | GEOLOGICAL FRAMEWORK

3.1 | Igneous and sedimentary setting

The San Rafael Volcanic Field is situated within the San Rafael Swell in southeast Utah, USA (Figure 1), which lies along the northwestern margin of the Colorado Plateau. The San Rafael Swell is composed of Precambrian igneous and metamorphic basement overlain by 3–5 km thick Phanerozoic sedimentary rocks (mainly Jurassic age) and Pliocene magmatic rocks (Reid et al., 2012; Thompson & Zoback, 1979). Magmatism was related to the crustal extension along the margins of the Colorado Plateau, due to slab rollback and lithospheric delamination during the Neogene (Humphreys, 1995; Tingey et al., 1991). This resulted in voluminous intraplate volcanism along the transition zone between the Colorado Plateau and the Basin and Range Province (Gonzales & Lake, 2017; Luedke & Smith, 1984).

The San Rafael Volcanic Field consists of a deeply eroded subvolcanic complex of alkaline sills and dykes, which intruded the San Rafael Swell around 3.4–4.7 Ma (Delaney & Gartner, 1997). Estimations based on Cenozoic erosion rates, the presence of vesicles in the intrusion, and the age of magmatism conclude that the emplacement depth was ~1 km (Díez et al., 2009; Germa et al., 2020; Pederson et al., 2002; Richardson et al., 2015). The San Rafael Volcanic Field has previously been described in several studies and is composed of approximately 200 dykes and sills of trachybasalt (e.g. Delaney & Gartner, 1997; Díez et al., 2009; Kiyosugi et al., 2012; Kjenes et al., 2023; Richardson et al., 2015).

The host rocks for the intrusions in the San Rafael Volcanic Field are composed of the Middle Jurassic sedimentary strata of the San Rafael Group (Delaney & Gartner, 1997; Gilluly, 1927). This succession was accumulated in a distal position of the Northeast-Southwest oriented foreland basin known as the Utah-Idaho trough (Bjerrum & Dorsey, 1995). Its conforming units, the Carmel, Entrada, Curtis, and Summerville Formations, are composed of clastic facies originated in shallow-marine to nearshore, paralic, and aeolian environments, and record several transgressions and regressions of the sea in the basin (Anderson & Lucas, 1994; Zuchuat et al., 2018).

The Entrada Formation constitutes the host-rocks in the studied outcrop. The entrada is characterized regionally by two stratigraphic units: (i) the Slick Rock Member, composed mainly of well-sorted and well-cemented, fine-grained sandstones, accumulated by a wet aeolian dune system (Crabaugh & Kocurek, 1993), and the overlying (ii) 'Earthy Facies' Member which is characterized by poorly cemented, fine-grained, moderately sorted silty and massive sandstones, interbedded with mudstones, gypsum and thin trough-cross bedded sandstone beds (Doelling et al., 2015; Peterson, 1988; Zuchuat et al., 2019). Only the Earthy Facies Member is found at the study area. Although several descriptions of the lithology of this member are documented, the sedimentary architecture of the Earthy Facies Member has been relatively understudied in comparison to the Slick Rock Member. The Earthy Facies succession is interpreted to have been deposited in a wet aeolian environment transitioning into supratidal- to shallow marine settings (Skurtveit et al., 2021). Given the general good sorting of the massive sandstone facies, it is likely that they are related to aeolian accumulation, either by migrating dunes and or by settling in a regularly damp or vegetated environment like a sand sheet (Gross et al., 2023). Silty mudstones that are found interbedded with these sandstones are likely the result of settling from aqueous suspension. This could be the result of wet interdune accumulation (sensu Kocurek, 1981), or it could be the result or wetter conditions in a sand sheet (Kocurek & Havholm, 1993). Heterolithic facies, in contrast, record the alternating action of accumulation by unidirectional currents of water, and by settling of silt and mud, with signs of subaerial exposure in the mudstones (Collinson, 2019).

Given the extensive (several kilometres) lateral continuity of the intervals, it is likely that the accumulation

of different facies was controlled by external parameters, such as changes in humidity and or water table level (Kocurek & Havholm, 1993). The massive sandstone and silty mudstone facies could be the result of dryer periods in which aeolian processes dominated, while the heterolithic facies could be linked to wetter periods, likely related to the expansion of supratidal flat/marine sabkha domains which are expected to become more prominent towards the northwest (Crabaugh & Kocurek, 1993; Gross et al., 2023).

4 | METHODS AND DATASET

The study area is composed of the eastern section of the Cedar Mountains (Figure 1), which is located within the San Rafael Volcanic Field in Eastern Utah, USA. This eastern section is divided into the southeastern locality and the northeastern locality (Figure 1). While the southeastern Cedar Mountain locality is 400 m wide and accessible for logging and sampling, the northeastern locality is much larger (3.5 by 0.16 km) but characterized by high and vertical cliffs only accessible to remote studies. Synthetic seismic modelling was carried out on the northeastern Cedar Mountain sill due to the lateral extent of the sill (i.e. width), which is comparable to dimensions of sills found in actual subsurface reflection seismic datasets (e.g. Gilmullina et al., 2021; Rohrman, 2013). Both locations were chosen for this study based on the accessibility of the outcrop and the length of the intrusion. Lateral variability is low for the sedimentary rocks, so the lithological observations in the accessible outcrop can used to interpret lithology from weathering faces in the larger outcrop. The lateral variability along the sill width on the other hand, is relatively high for the sill intrusion. Sills emplaced within Cedar Mountains are observed parallel to propagation (ENE-WSW). All models and images are oriented perpendicular to magma propagation (N-S), which implies that magma propagation is towards the camera.

The outcrop models use data acquired using a 'DJI Mavic 2 Pro' UAV with a 28 mm lens, which gathered data and by flying at a constant distance (ca. 20 m) with a perpendicular view of the cliffs. Preplanned mapping was not used, due to the curving nature of the cliffs, and all images were collected by manually flying the drone. 1364 images containing full GPS- and altitude metadata were collected with ca. 70% overlap. These images were further processed with *Agisoft Metashape* to create the three-dimensional models. Processing steps include alignment of images, point-cloud editing and decimation, triangulation of the points to create the mesh for the topographic model, and texturing of the model with selected images (e.g. Mitten et al., 2020). Errors were accounted for by using Agisoft's gradual selection tool for reprojection error, reconstruction uncertainty, and projection accuracy. This resulted in multiple models with ground pixel resolution ranging from 1.12 to 3.96 cm/pixel and a reprojection error of 0.46–0.70 pix.

Three sedimentary logs with a total length of 60 m were collected from the southeastern Cedar Mountains locality which is accessible for study (Figure 1). These record grain size, lithology, sedimentary structures, and sill contacts and were used to define key lithology types or 'lithofacies' that can be correlated to their expression in outcrop. The larger northeastern locality (Figure 6) is too high to be accessed and could only be investigated in the virtual outcrop models. The sedimentary logs were applied to the virtual outcrops, making it possible to interpret in which sedimentary interval the sills were emplaced. The sedimentary logs and virtual outcrops were used to recreate the sedimentary strata above the intrusion. This was performed by translating the sedimentary strata from beneath the base of the igneous intrusion to the top of the intrusion. The recreation of original strata was completed by assuming pure inflation of the emplaced sills. In this scenario, the underlying stratigraphy is assumed to have been directly uplifted and the lateral continuity of the lithological layers was constant at the time of emplacement.

Synthetic seismic models used in this study yield data that stimulate zero-phase, pre-stack depth-migrated (PDSM) reflection seismic data (Lecomte et al., 2015), and this was achieved through a workflow using Matlab and SeixRox which is explained in more detail in Eide et al. (2018). Four main parameters are important for the synthetic seismic modelling used in this study: rock P-wave velocity, rock density, seismic frequency at target depth, and maximum imageable dip of strata (max dip at target depth). These parameters vary greatly in real seismic datasets and are dependent on the depth of modelling target, geological history and overburden of the target, and overburden architecture (Eide et al., 2018). Consequently, synthetic seismic models for both 30 and 45 max dips are presented to investigate differences in seismic models caused by overburden. For instance, intrusions with simple overburden often have a high max dip (and high lateral resolution) at shallow depths and decrease rapidly to ca. 45° at 3 km depth (Eide et al., 2018). Intrusions with complex overburden, such as high velocity layers above the target, lead to much lower horizontal resolution and a max dip of 30° at 3 km depth. Values of the properties in this study were copied from Eide et al. (2018), which applied P-wave velocity and host rock density from relevant depths in time-equivalent formations from the Norwegian Continental Shelf. P-wave velocity and density of the igneous intrusions were found in Smallwood and Maresh (2002) (Table 1). In principle, mafic igneous intrusions emplaced into sedimentary host rocks are easily identified in seismic datasets due to the high

density and velocity contrasts between mafic intrusions and sedimentary host rocks (Eide et al., 2018; Smallwood & Maresh, 2002). However, issues related to seismic imaging typically occur due to three inherent limiting factors:

(i) Decrease of seismic quality and resolution with depth due to absorption of high frequencies, seismic energy, and downward increase in seismic velocity (e.g. Thomson & Hutton, 2004).
(ii) Overburden effects, where the seismic signal is affected by complex overburden (i.e. overlaying intrusions or complex host rock layering), which can be considerable problem in basins with igneous rocks (e.g. velocity pull-ups, seismic blanking) (Eide et al., 2017; Flecha et al., 2011; Fliedner & White, 2003; Gallagher & Dromgoole, 2007; Holford et al., 2012; Planke et al., 2018).
(iii) The inability of the reflection seismic method to image steeply dipping and vertical interfaces (Eide et al., 2017, 2018; Lecomte et al., 2016).

To investigate some of these limiting factors on the imaging of sill architecture and sill marginal features, the northeastern Cedar Mountains locality has been modelled using seismic frequencies of 20 and 30 Hz and maximum imageable dip of strata and lateral resolution of 30°–45°. The seismic frequencies were chosen based on the typical burial depth of sills in the literature (sensu Eide et al., 2018), where a frequency of 20–30 Hz roughly translates to a target depth of ca. 3 km. This is vastly controlled by the overburden and presence of high-velocity layers above the intrusions.

5 | RESULTS

Two locations are further discussed in this subsection: the southeastern- (Figures 3–5) and northeastern Cedar Mountains (Figures 6 and 7). The southeastern Cedar Mountains locality provides a detailed view of the emplacement of the sill, while the northeastern Cedar Mountains shows multiple kilometres of sills intruding through different units of the Entrada Formation, thus facilitating the acquisition of a large amount of numerical data making a quantitative study possible.

Both localities feature the Earthy Facies of the Entrada Formation, thus ensuring that descriptions of the sedimentary units made in one locality are also valid for the other. Three logs were collected in the Southeastern Cedar Mountains (Figures 3 and 4) which were used to interpret the sedimentary units in the Northeastern Cedar Mountains (Figure 6). The host rocks consist of poorly cemented, layered, sandy heteroliths (interbedded sandstone and mudstone beds), mudstone and massive sandstone from the 'Earthy Facies' of the Entrada Formation. A lesser amount of the rock volume also comprises laterally extensive mudstone units from the same formation. Sills are emplaced within all these units but appear to intrude mostly within the heteroliths. It is hard to provide an absolute observation of this due to the extensive alteration of the sedimentary host rocks in the close vicinity of the sill. The alternated host rocks feature a change in colour, from reddish brown to pale yellow (e.g. Figures 3 and 5). The sills found in the Cedar Mountains have an average thickness of 18 m and are thin towards the northwest (Figure 3). The sills consist of alkaline basaltic with an aphanitic crystal texture. Sill margins generally have finer grain sizes and appear sharp. Host rock in contact with the sill shows a pale discoloration ca. 6–280 cm away from the sills in the Southeastern Cedar Mountains locality and 0.9–5.2 m in the Northeastern Cedar Mountains. Two dykes are observed in this area crosscutting the sill. However, the dykes are not mapped in detail and they are not used for the synthetic seismic.

5.1 | Southeastern Cedar Mountains

5.1.1 | Sedimentary lithofacies

The three sedimentary logs (Figure 4) were acquired along the exposed sill with a spacing of 120–200 m (Figure 3). Three lithofacies were observed: (i) massive sandstone, (ii), heterolithic facies consisting of interbedded sandstone and mudstone and (iii) silty mudstone (Figure 5).

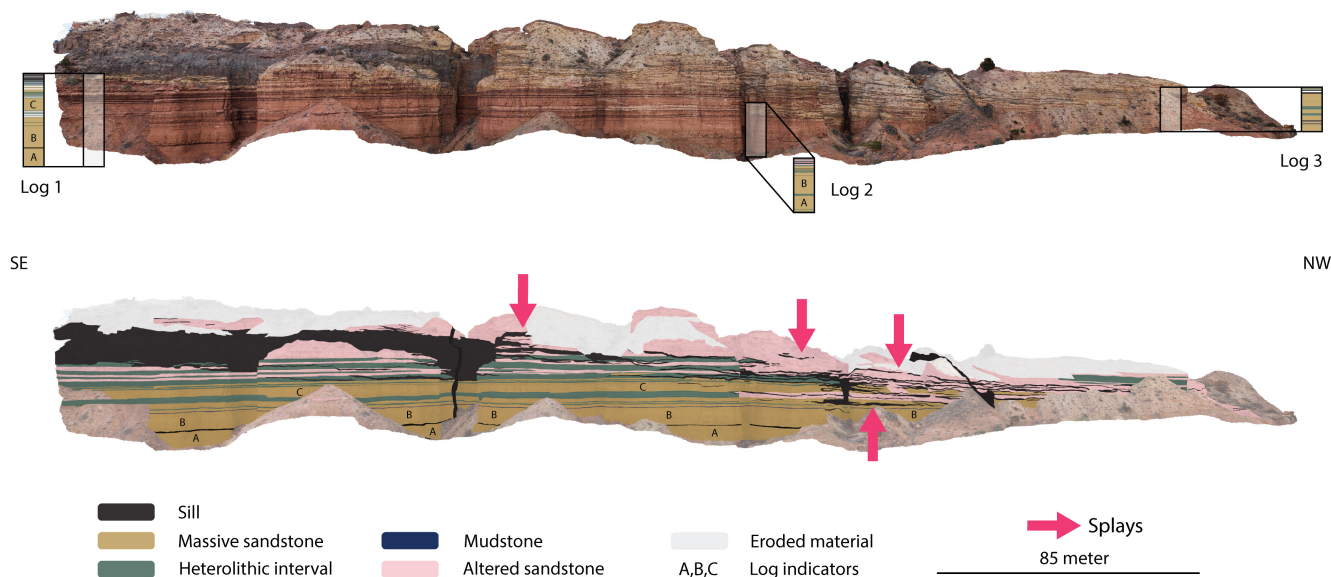(i) Massive sandstone facies are characterized by fine grain size, good sorting, light red colour, and an

TABLE 1 Input data for modelling (modified after Eide et al., 2018).

Facies	V_p (km s^{-1})	V_p/V_s fraction	Density (g cm^{-3})	Source NCS well/article
Igneous intrusion	6.3	1.86	3	Smallwood and Maresh (2002)
Mudstone	3.8	1.80	2.5	6407/2-1
Heterolithic	3.3	1.80	2.3	6407/2-1
Sandstone	3.5	1.80	2.4	6407/2-1

FIGURE 3 UAV model of the Southeastern Cedar Mountains Locality and schematic interpretation of the outcrop. This schematic features sills (dark grey), massive sandstone (yellow), heterolithic intervals (green), mudstone (blue), and bleached lithology (pink). Thick layers that are recognized have been given a letter (A, B and C) for easier correlation between the logs.

apparent absence of sedimentary structures. Bed boundaries appear to diffuse within massive sandstones and form 0.4 to 7-m-thick intervals overlying and underlying other lithofacies. Towards the top of these successions, it is common to see a more intense red tone, poorer grain sorting along with a silty and indications of bioturbation. This is also common when the sandstones are thinner (<1 m thick). Some of these sandstones are characterized by the presence of thin anhydrite veins aligned parallel to each other and dipping at low angles with respect to the top and base of the successions (Figure 5e). Massive sandstone facies are the most common lithology occurring in the Southeastern Cedar Mountains locality and they make up approximately 40% of the photogrammetric model of the outcrop including sills.

(ii) Heterolithic intervals consist mainly of interbedded light-red sandstone and dark-red mudstone in different proportions. Sandstone beds are typically 3–20 cm thick, have sharp and planar bases and sharp and planar to convex-up tops (Figure 5a). Internally they either display low-angle cross lamination and ripple-scale cross lamination or are massive. Mudstones are usually massive and appear to form blocky or subangular blocky aggregates. Anhydrite veins are present in some of the heterolithic intervals and may crosscut the interbedded layers. Heterolithic intervals are typically around 1 m thick, and they are usually interbedded with thin (40–50 cm thick) massive sandstone facies. These facies make up 20% of the outcrop.

(iii) Silty mudstone facies are dark red in colour and usually massive (Figure 5c). Their thickness ranges from

5 to 60 cm, while ca. 10 cm is the most frequent. In contrast to the heterolithic facies, these mudstone intervals are found between thick (at least 0.4 m) massive sandstone facies. These facies are the least frequent lithology at the Southeastern Cedar Mountains locality, constituting approximately 10% of the outcrop.

The described facies are laterally continuous at the outcrop scale. They form intervals that can be directly traced across the 3 logs in the south-eastern sector with the help of the virtual outcrop model (Figure 3). The same occurs in the northern sector in which intervals are easily traceable and continuous across ca. 4 km in a roughly N-S direction (Figure 6).

5.1.2 | Sill characteristics and geometry

The sills interpreted in the Southeastern Cedar Mountains outcrop show high lateral thickness variability from southeast to northwest and are 0.2–10 m thick. They appear either as a single thick sill or multiple splays occurring at different horizons (e.g. Figure 3). The sills are emplaced in all lithologies, but often feature bleaching (i.e. thermal alteration) of the host rocks. However, this issue is countered by tracing the host rocks laterally away from the sills. The most apparent contact of sill and host rock appears to be within the heterolithic intervals, more specifically at the contact between interbedded sandstone and mudstone (Figure 5a,b). The heteroliths often feature multiple splays emplacing along different horizons. Sills splays are observed within the silty mudstone layers (Figure 5b–d),

FIGURE 4 Lithology of the Entrada Formation, divided into three logs (see Figure 3 for locations). Observations and interpretations should be noted next to the log. The general patterns observed in this log are also valid for the rest of the study area. The letters A, B and C correspond to easily distinguishable beds found in the virtual outcrop model for the Southeastern Cedar Mountains locality (Figure 3).
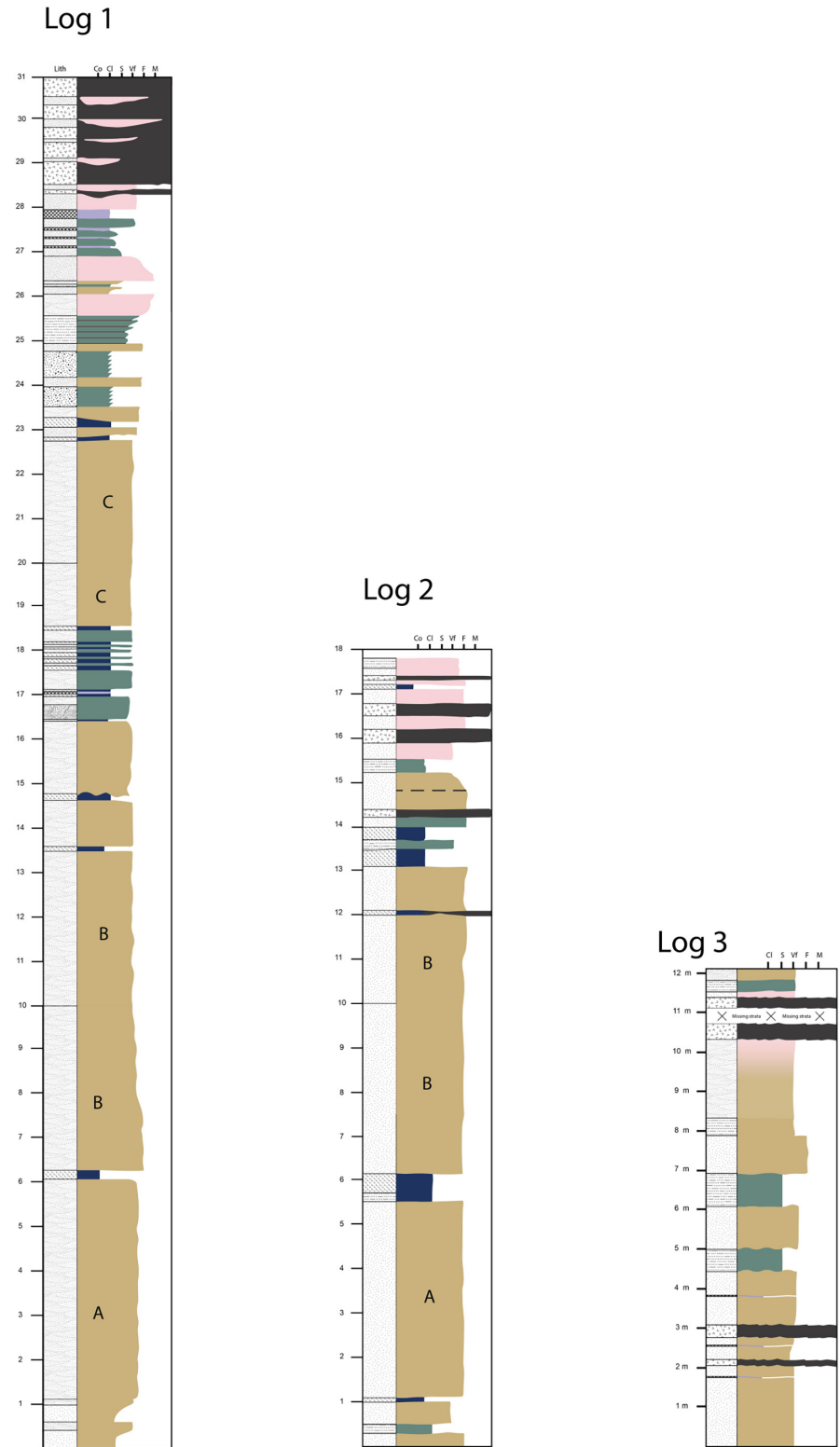
along with anhydrite veins. The base and top contact between the sills and host rock appear to be influenced by anhydrite veins, similar to the case for the heteroliths. As shown in Figure 5d, anhydrite veins appear deformed in front of the sill splay in a ductile fashion. No lateral shortening by thrust faulting and/or folding of host rock layers are observed, or imbricated stacks of repetitive lithology.

The sills are also found emplaced within massive sandstone layers (Figure 5f). The massive sandstone may also exhibit anhydrite layers, but they may also emplace without exploiting anhydrite veins as shown in Figure 5f. In this case, the sills emplace within local discontinuities in the host rock, which is shown by the flat geometry of the sill splay.
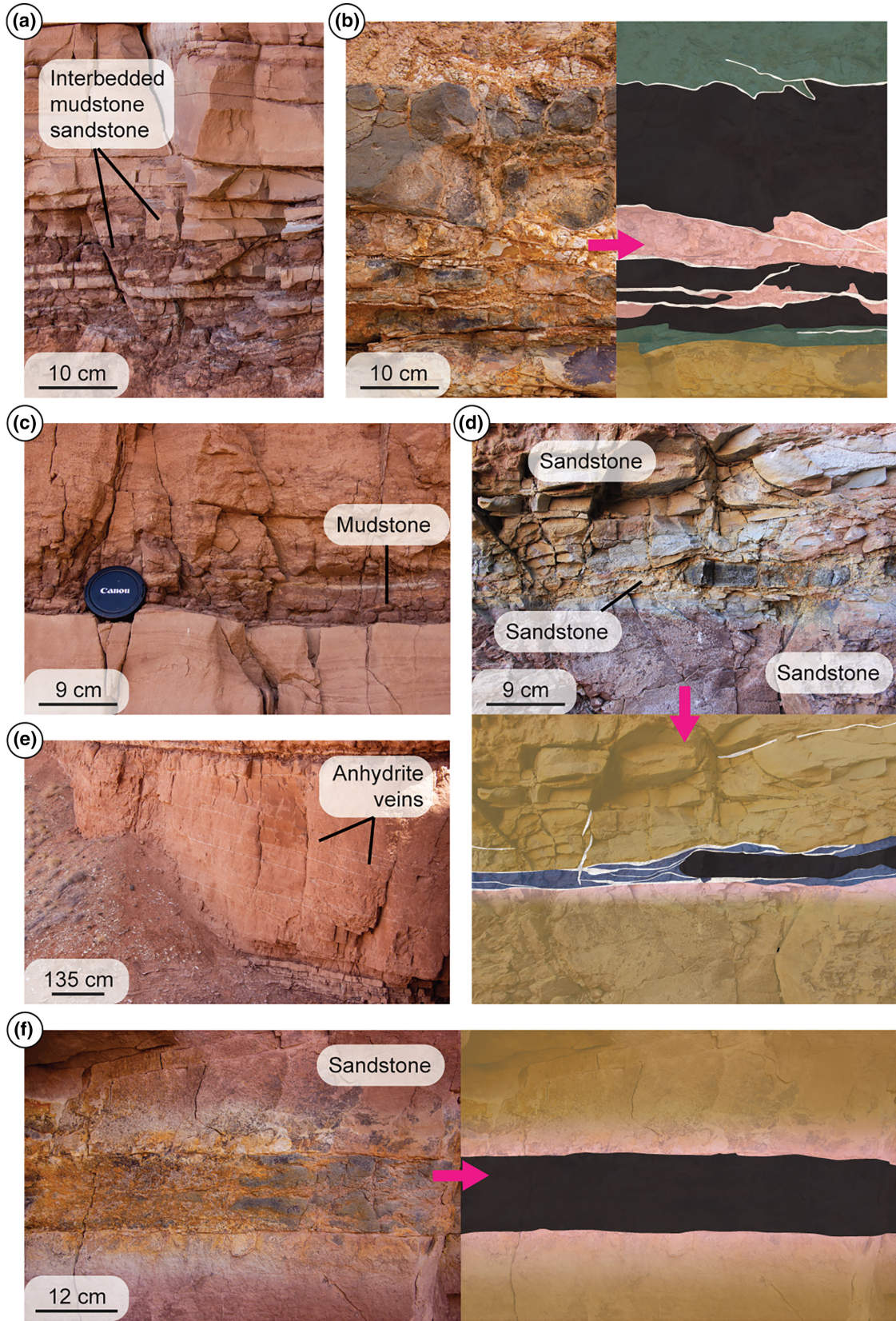
FIGURE 5 Figure showing the lithological relationship between sills and the Entrada Formation. (a) Shows a picture of a typical section of heterolithic intervals with interbedded sandstone (light red) and mudstone (dark red) layers. (b) Shows three sills (dark grey) that are emplaced within a similar heterolithic layer (green) which is featured in (a). (c) Shows a typical mudstone layer (dark red) on top of a massive sandstone layer (light red). (d) Shows a sill splay (dark grey) intruding within a mudstone layer (blue). (e) Field photo of a typical massive sandstone bed. The thin white lines are anhydrite. (f) Image and interpretation of a sill (dark grey) intruding within a massive sandstone layer (yellow). The contact between the sill and host rock features a more yellow-ish colour, which indicates the bleaching of the host rock (pink).

5.2 | Northeastern Cedar Mountains

The Northeastern Cedar Mountains locality is a 3.5-km-long (orthographic measurement) cliff face located within the San Rafael Volcanic Field (Figure 6). This locality is described by one large three-dimensional model, featuring five smaller models of sills emplaced within the Entrada Formation. Previous studies have concluded that the sills in Cedar Mountains are of alkaline basaltic origin (e.g. Germa et al., 2020). The intruded interval has a 150-m difference in vertical position from south-southeast to north-northwest in the cliff face (elevation data from *Google Earth*). Three main sill segments are recognized in the outcrop by looking at the overall geometry of the sill contacts and correlating this with one broken- and unbroken bridge with a vertical jog of ca. 15 m (Figure 6). The first segment, Segment A (Figure 6a,b), shows undulating morphology which moves down in lithology from north-northwest to south-southeast (Figure 6b). Most of this segment appears to have been emplaced within massive sandstone and is approximately 750 m wide and shows a total vertical jog of 40 m. The second segment, Segment B (Figure 6a,b), has mostly been emplaced within the same heterolithic interval and features an overall layer-parallel geometry. This segment is approximately 900 m wide and features some minor vertical jogs down towards the south-southeast (Figure 6). The third segment, Segment C (Figure 6a,b), is similar to Segment B and is also emplaced more or less within the same heterolithic interval. However, this differs from Segment B due to a vertical offset between sill segments of ca. 10 m. This segment is approximately 1850 m long and features some vertical jogs both up and down in stratigraphy. The general trend in the geometry of the major sill segments appears to be transgressive from the northern to southern tip of the Northeaster Cedar Mountains cliff (Figure 6). This is highlighted in the morphology profile provided in Figure 6b, in addition to the number of magmatic bridges. There are 44 broken- and 4 mapped unbroken bridges with a vertical offset less than 10 m, which highlights the complexity of the sills within the Entrada Formation. Furthermore, eight minor sill segments are observed within the three major segments in northeastern Cedar Mountains and are distinguished by either broken or unbroken bridges with vertical jogs larger than 10 m (Figure 6b).

The main sills show a thickness of 13–22 m (Figure 6c), while the thinner splays have a thickness of 2 m or gradually decreasing until terminated. The thicknesses of the sills are measured where the sills exhibit a clear top and bottom contact to the host rocks, which is relatively rare along the contact. Only 1 km out of the total 3.5 km exhibit a preserved sedimentary top contact. The thickness measurements are plotted as a red graph in Figure 6c. These measurements are further plotted to create a mean thickness, which is indicated by the dark blue graph in Figure 6c.

Even though most of the original lithology above the sills have been eroded away, we can recreate the original stratigraphy by assuming pure inflation of the emplaced sills. In this scenario, the underlying stratigraphy is assumed to have been directly uplifted and the lateral continuity of the lithological layers was constant at the time of emplacement. The base contact between the sills and the host rocks was extrapolated by interpreting the entire base contact of the sills and checking if the sills had emplaced at either the boundary between two lithologies or within one lithological unit. The results, as shown in Figure 6d, indicate that the heterolithic intervals are the lithology with the highest concentration of sills at 52%. Approximately 23% of the sills occur within the massive sandstone, while 25% of the sills are emplaced within mudstone (Figure 6d). The sills geometry is traditionally layer-parallel if emplaced within heteroliths or mudstone, as illustrated in Figure 7a,b. Both sills and sill splays typically transgress over short vertical distances (i.e. change stratigraphic interval) if emplaced within the massive sandstone units (Figure 7c).

The highest proportion of sills base contacts is observed within the heterolithic intervals (ca. 52%) at Cedar Mountains. The sills are often emplace within a heterolithic interval and move up and down within the same interval (as shown in Figure 6a) and not following a single horizon. The contact of the heteroliths and the sills is mainly sharp and appears locally transgressive. Most of the sills in this lithology appear strata-bound (Figure 7a). Smaller vertical offsets of bridges in heteroliths are limited to a few meters with multiple splays developed around the base boundary of the sill. A total of 35 broken- and 4 unbroken bridges are found within the heterolithic intervals
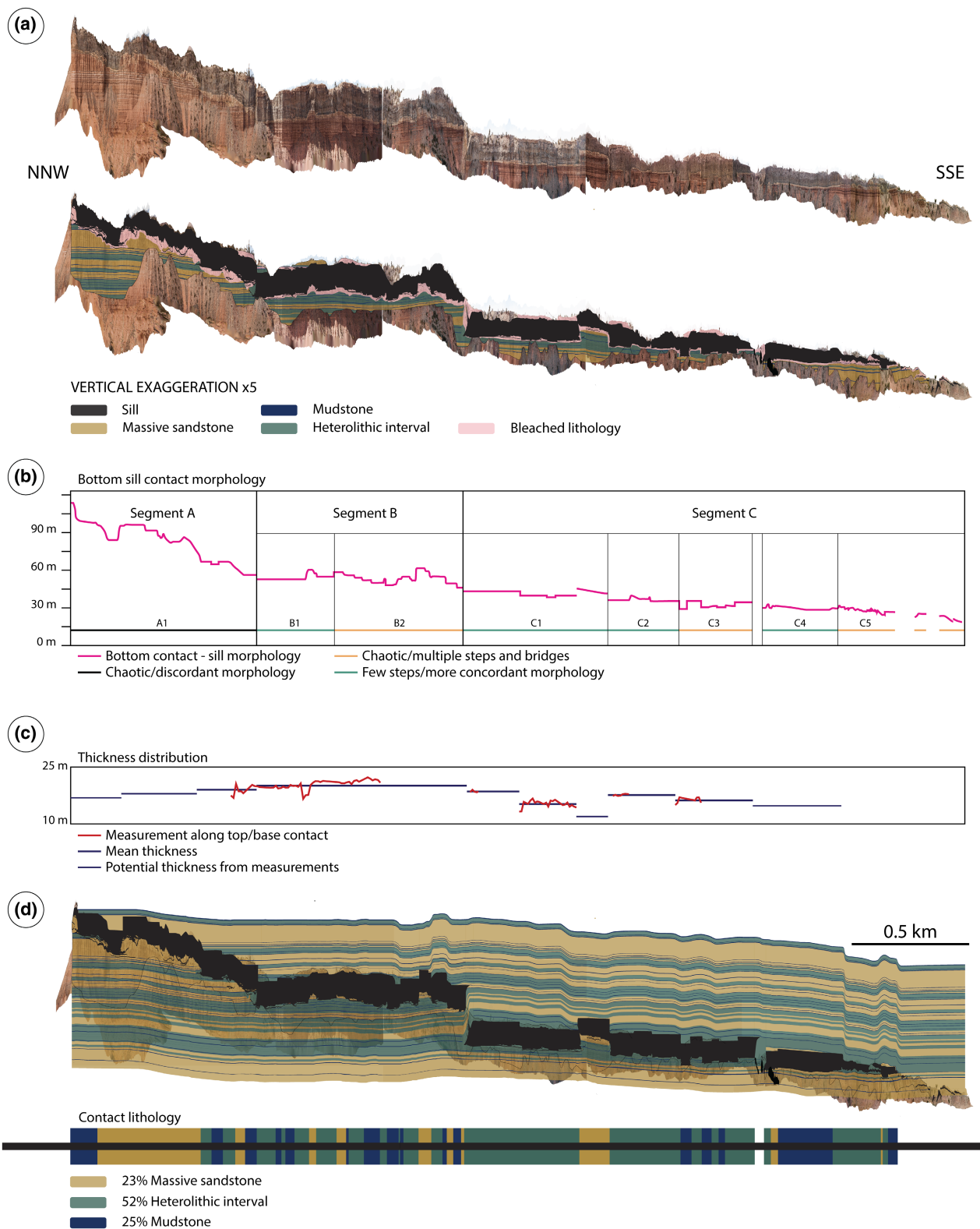
FIGURE 6 Overview of the Northeastern Cedar Mountains locality. The model has an increased vertical scale of 5 to better visualize the sills and lithology. (a) This features a stitched three-dimensional model and corresponding interpretation. (b) The sill geometry graph shows the true geometry of the base contact between the sill and the lithology, with both measured geometry (pink lines) and segment division (blue lines). (c) The thickness distribution features the true sill thickness (pink lines), mean thickness values from measured thickness values and potential thickness measurements based on simple linear regression. (d) Simple recreation of original overburden, based on both simple inflation and local lithology that are missing. This reveals which layers the sills were originally emplaced in.
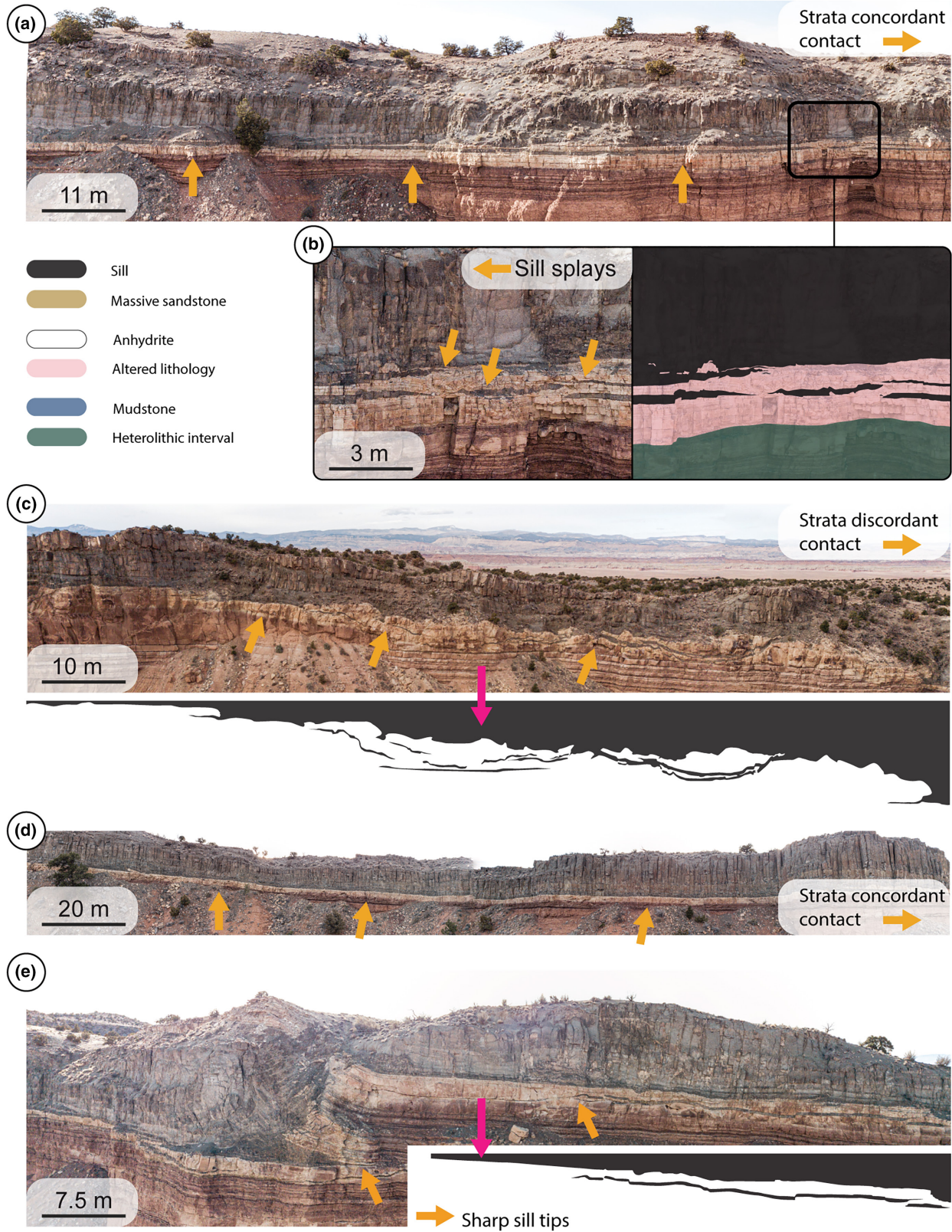
FIGURE 7 Field images acquired with a drone of bridges and base contact between the sill and host rocks. (a) Shows a planar contact between the heterolithic interval and the sill. Some minor splays occur beneath the base of the sill. (b) Close up of the splays beneath the base of the sill. Bleaching stops at the mudstone boundary. (c) Planar, concordant contact between the sill and a mudstone interval. (d) Strata discordant base contact between the sill and massive sandstone. The sketch shows the complex base contact. (e) Photo showing a large bridge and sharp sill tips of splays beneath the base of the sill.

and have an average jump of 1.5 m, ranging from 0.3 to 5 m.

About 23% of the sills base contact is emplaced within the massive sandstone layers and commonly show splays, bridges, and often climb through their respective layers (e.g. Figure 7c). The contact between the massive sandstone and the sills is sharp and locally irregular due to the transgressive nature of the sills and splays. However, the contact between sills emplaced and host rock is sharp and may follow this discontinuity for long distances. This is shown in Figure 7d where the sill follows a discontinuity between massive sandstone and mudstone for 220 m before it ends in a broken bridge with an ongoing splay in the same interval for another 55 m. About 10 broken bridges are found within massive sandstone, featuring an average stratigraphic jump of 3 m, ranging from 0.7 to 10 m.

About 25% of the sill base contact is emplaced within the mudstone intervals at Cedar Mountains, even though the host rock is the least common in the Cedar Mountains. The contact of the sills with host rock commonly shows a sharp and featureless margin and exhibits much sparser bridges and transgressive splays than sills propagating in both heteroliths and massive sandstone. The sills appear to not follow individual mudstone layers for larger distances, as they tend to only follow them for approximately 10–17 m. Often sills transgress to other discontinuities from mudstone layers through bridges, and an arrested sill splay is situated within the mudstone layer.

The host rocks in the Northeastern Cedar Mountains feature the same type of bleaching that was observed at the Southeastern Cedar Mountains locality (Figures 6 and 7d). The zone of bleaching near intrusions varies in thickness from 6 to 280 cm away from the sills in the southeastern Cedar Mountains locality and 0.9–5.2 m in the northeastern Cedar Mountains. Sedimentary logging and thin section analysis reveal that the unbleached Entrada sandstones show the presence of haematite grain coating of quartz in addition to chlorite and oxides in the matrix. However, the bleached zones lack haematite grain coating.

5.3 | Synthetic seismic modelling

Synthetic seismic modelling was performed using the interpreted outcrop model presented in Figure 6d as input. Frequencies of 20 and 30 Hz were chosen in addition to the maximum imaged dip angle of 30° and 45°. This resulted in four different scenarios which share some similarities, but also feature key differences of imageable details related to the sill. This synthetic seismic dataset is used to observe which marginal features (i.e. broken bridges, splays, etc.) fall beneath seismic resolution. In addition, compartmentalization is investigated by comparing

visible sill geometries in the synthetic seismic with the high detailed virtual outcrop.

First, all synthetic seismic models presented in this study lack clear reflectors representing the bedding of the host rock (Figure 8), because the sedimentary layers have low impedance contrasts compared to the sill and are very thin compared to the seismic resolution of 27.5 m (for 30 Hz) (Table 1). The igneous intrusions, on the other hand, have P-wave velocities and densities much higher than the surrounding host-rocks and occur as high-amplitude reflectors. These reflectors from the igneous intrusions are 'tuned', meaning they are imaged as a single reflector as they are too thin to be imaged with a separate top and bottom reflection (e.g. Kallweit & Wood, 1982). However, the sedimentary bedding is more visible at 30 Hz resolution compared to 20 Hz (Figure 8). No difference for the relatively planar host-rock bedding was observed by comparing the maximum imageable dip.

The igneous intrusions appear to have consistent high-amplitude reflectors apart from Segment C5. Here, a clear amplitude decrease towards the right is apparent, which reflects a clear rightwards decrease in sill thickness (Figures 6d and 8). This reduction in reflection amplitude is consistent in all synthetic seismic models, indicating a good correspondence between sill thickness and reflector amplitude for sills that are thinner than the tuning thickness. This, however, involves the assumption that the sill thickness is below the maximum tuning thickness (e.g. Eide et al., 2018), which is the case for our dataset. The sill thickness in C5 is measured to ca. 15 m while the maximum tuning thickness is measured to 55 m for 30 Hz frequency and 41.25 m for 20 Hz. The virtual outcrop data, which the synthetic seismic dataset is based on, also show thinning towards the same direction as the amplitude decrease (Figures 6d and 8).

All three major sill segments are distinguishable in both the 20 and 30 Hz models, but the amount of detail observed within these major segments varies greatly. The broken bridge between major sill Segment A and B appears as a continuous reflector for all synthetic seismic models and is therefore well imaged. However, the unbroken bridge between major sill Segment B and C only appears as a discontinuous reflector for the 30 Hz resolution models (Figure 8). It does appear as a semi-continuous reflector within the 20 Hz model with a 45° max dip, but it is not apparent that this is an unbroken bridge from the synthetic seismic data. The general geometries of the major sill segments were found by importing synthetic seismic models into Petrel and interpreting the sill reflectors by using autotracking. All three major sill segments are recognizable and well-imaged in the synthetic seismic models. Major sill Segment A appears as a discordant reflector with little to no apparent difference
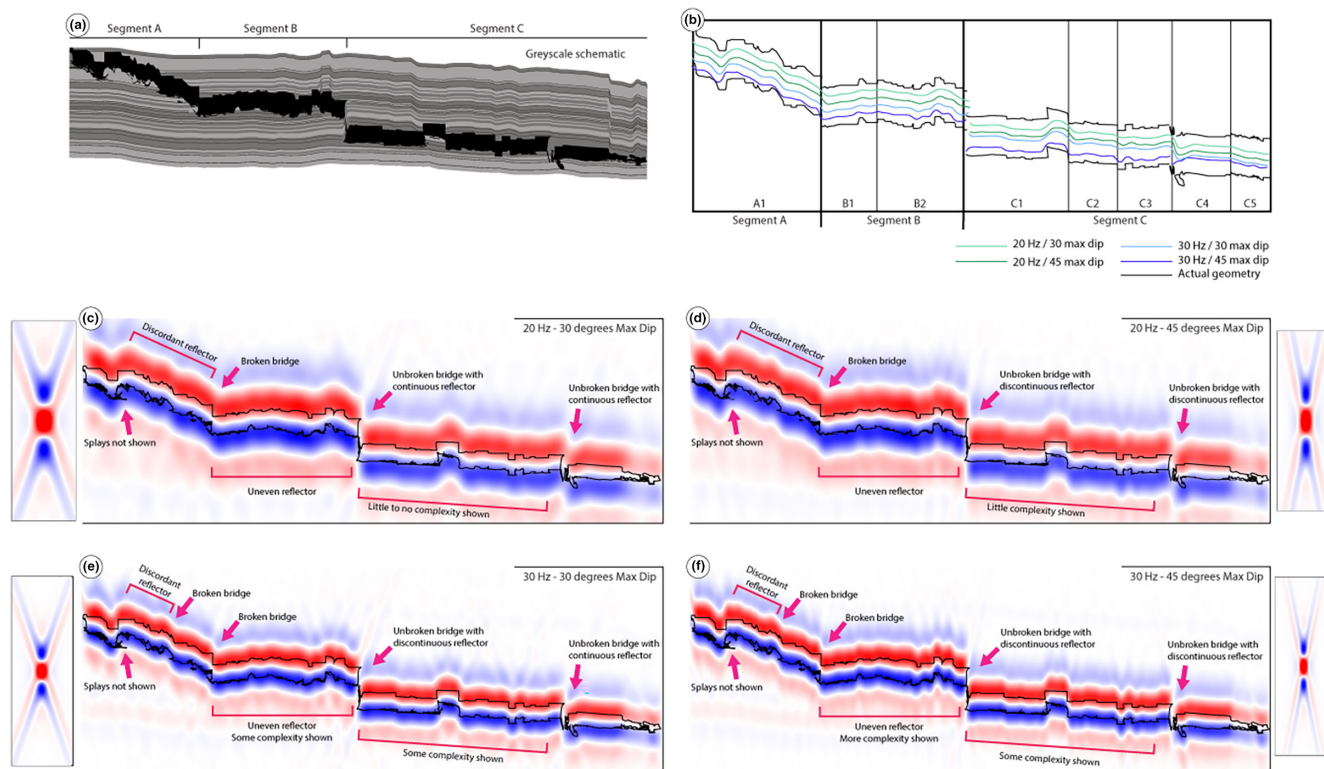
FIGURE 8 Synthetic seismic models created in SeixRox. (a) Outcrop data from northeastern Cedar Mountain in greyscale. (b) Interpreted base boundaries of the sill. The black lines represent the base boundary interpreted from the three-dimensional field model, while green lines represent base boundaries interpreted in Petrel with autotracker for 20 Hz, while blue lines represent base boundaries interpreted in Petrel for 30 Hz. (c) Synthetic seismic model with 20 Hz and 30° maximum dip. (d) Synthetic seismic model with 20 Hz and 45° maximum dip. (e) Synthetic seismic model with 30 Hz and 30° maximum dip. (f) Synthetic seismic model with 30 Hz and 45° maximum dip.

between the two seismic resolutions and corresponding maximum imageable dips. Major sill Segment B and C appear as layer concordant intrusions with variable detail in terms of morphology. In general, sedimentary bedding is difficult to observe due to the density contrasts between igneous intrusion and the host rocks. However, the general impression of bedding can be traced by observing the overall bedding attitude of the large-scale stratigraphic framework that is imaged. This is typically interpreted based on formation boundaries or stratigraphic discontinuities.

The sill morphology that is possible to deduce from the maximum amplitude of the synthetic seismograms is presented in Figure 8b. In general, the highest seismic resolution and max dip provide the most detailed insight into the true distribution of bridges and steps within the major sill segments. This is evident by comparing the geometry of the synthetic seismic models with the interpreted sill morphology from the field analogue (Figure 8). Bridges and steps are represented by changes in height of the interpreted line (i.e. change of vertical stratigraphic unit) or vertical jogs. About 53 jogs occur in the field outcrop (Figure 6). Most of these discontinuities are not distinguishable in the synthetic seismic because of limited

seismic resolution. All 3 major bridges (≥15 m vertical jog) are recognized in the synthetic seismic data, while the eight minor sill segments (≥10 m vertical jog) are not possible to delineate in all datasets. An example of this is the unbroken bridge between Segment C3 and C4, which appears as a continuous reflector for both 20 and 30 Hz resolution with a max dip of 30° (Figure 8) and 45° max dip for 20 Hz, but is visible as a discontinuous reflector for 30 Hz resolutions with a max dip of 45° (Figure 8).

In all these model realizations, sill features that show a displacement of less than 10 m are difficult to detect in our synthetic seismic dataset. None of the splays around the sill are observed within any of the synthetic seismic models, most likely due to masking by the strong reflector from the main sill body, which is only 2 m away, compared to the seismic resolution which is 27.5 m for 30 Hz frequency and 41.25 m for 20 Hz frequency (by the $\lambda/4$ criterion). The reflectors of the splays, similar to the sedimentary layers, are too thin to be imaged with a separate top and bottom reflection or at all. An exception could be argued for the splays between the unbroken bridge between major sill Segment B and C. The 20 Hz synthetic seismic models exhibit a weak reflector between these two segments, similar to the weaker signal at Segment C4.

6 | DISCUSSION

6.1 | Potential link between sill geometries and host rock lithology

This study has thoroughly investigated a total of 3.5 km of sills emplaced in heterogenous sedimentary units, consisting of three different lithologies: massive sandstone, heterolithic intervals, and mudstone. Almost half (52%) of the sills base contacts are emplaced within heteroliths, 23% in massive sandstone, and approximately 25% in mudstone intervals (Figure 9a). These findings suggest that the sills in the San Rafael Volcanic Swell preferentially emplace within layered heterogenous host rocks, such as interbedded sandstone and mudstone. However, there is a clear difference in the abundance of these different lithologies in the outcrop. By calculating the proportions of different facies in the outcrop, we find that sandstone and heteroliths are present in almost equal amounts, while mudstone is present in very small amounts (Figure 9b). This calculation is based on the present-day outcrop and not the recreated cross section. Thus, sills are overall 3.7 times more likely to be emplaced in mudstone layers than in the other two lithologies and least common within sandstone (Figure 9c). Mudstones are most likely intruded due to their low fracture toughness and strong anisotropy (e.g. Mudge, 1968). These properties allow the sills to part the mudstone layer itself along preexisting weakness planes and propagate through the mudstones (Eide et al., 2017; Kavanagh et al., 2006). Although the mudstone layers in the Entrada Formation are cemented, the sills appear to have no difficulty splitting and propagate through them. The following subsections will discuss sill propagation

with respect to how the overall emplacement changes during propagation through different sedimentary lithologies.

6.1.1 | Sill emplacement and geometry in mudstone

Even though the mudstone layers only make up 7% of the sedimentary host rocks in Cedar Mountains, 25% of all sills share a contact with this unit (Figure 9). This implies that the sills exhibit a relative probability of 370% (Figure 9) to be found within mudstones, compared to both heterolithic and sandstone intervals. Mudstones exhibit low fracture toughness and strong anisotropy, which makes them prime candidates for sills to propagate in. This corresponds with previous studies, which suggest that magma exploits mudstones due to zones of weakness and parting horizons along the emplacement direction of the intruding magma (e.g. Eide et al., 2017; Kavanagh et al., 2006; Mudge, 1968).

The sills within the mudstone layers exhibit slightly blunted tips (e.g. Figure 5d), which are typically associated with non-brittle emplacement of sills, such as during brittle and ductile faulting emplacement type sills (e.g. Spacapan et al., 2017). Blunted sill tips are traditionally associated with substantial inelastic deformation (e.g. Spacapan et al., 2017), which is not the case for the sills found emplaced within in mudstones Cedar Mountains. We can observe buckling, or bending, of the anhydrite in front of the sill tip (Figure 5d) and the presence of vertical fractures within the host rocks above the sill tip. These processes suggest that the sills emplaced in mudstones conform to linear elastic fracture
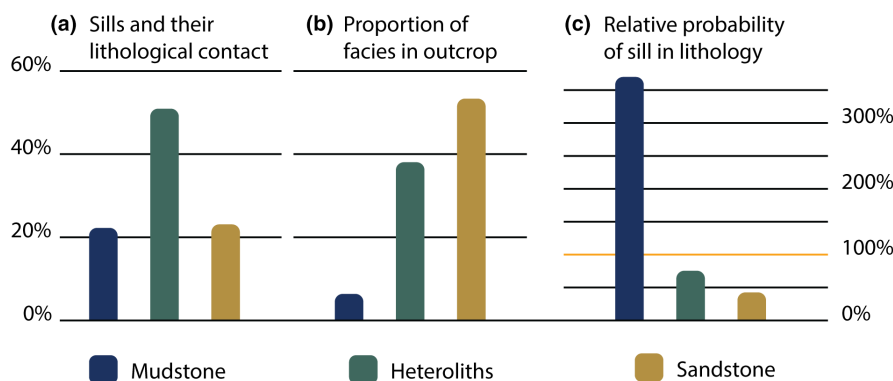

FIGURE 9 Statistical data derived from the base contact between the sill and host rocks (see Figure 6). All calculations are based on surface area from the three-dimensional models and associated interpretations. (a) Shows graphs and calculations for the amount of contact between sills and mudstone (25%), heterolithic interval (52%) and sandstone (23%). (b) Shows the proportion of the different facies in the outcrop which is mudstone (7%), heterolithic (39%), and sandstone (55%). (c) Shows relative probability which is calculated based on contact area between sills and respective host rocks and proportions of the facies in the outcrop. The results in a probability of sill intrusions in mudstone (369%), heteroliths (75%), and sandstone (43%).

mechanics. However, this moderately contradicts the observed blunted tips, which are commonly associated with non-brittle emplacement. An explanation may be that the sills develop blunted tips due to a halt in propagation. Thus, the tip cavity in front of the sill disappears, and the magma pressure can bend and deform the host rock and even widen the intrusion tip (Rubin, 1993; Spacapan et al., 2017).

The proposed mechanism is therefore that the sill splay emplaces within the mudstone due to its strong anisotropy and low fracture toughness as a thin, magma-filled fracture. During propagation, the splays become arrested or stop propagating and evolve blunted tips as the splays inflate. Furthermore, this results in elastic bending of the overburden due to inflation, which is accommodated by vertical fractures above the sill.

6.1.2 | Sill emplacement and geometry in massive sandstone

Approximately 23% of the sills base contact with massive sandstone, in which sandstones make up 55% of the host rocks in the northeastern Cedar Mountains. This implies a 43% relative probability of sill emplacement in sandstones. The overall sill emplacement is dominated by brittle fracture processes, which is expressed through the presence of bridges and step structures (e.g. Figures 6b and 7c,e). For example, the sill in Figure 7a,c has a planar, strata-concordant base boundary with the heterolithic host rocks, while the sill in Figure 7d is emplaced within massive sandstone and exhibit a complex strata-discordant base boundary. In general, sandstones exhibit higher tensile strength and lower anisotropy compared to mudstones (e.g. Zhai et al., 2021; Table 1), and will potentially be more resistant to the splay. This is evident in the Cedar Mountain sills as they do not appear to stay and follow single sedimentary sandstone beds in a planar and parallel manner, but display complicated morphologies where sills step up, step down, and cross-cutting stratigraphy (Figure 7d). This might be a result of a lack of strong lithological contrast within the sandstone layers for the sills to exploit or follow, resulting in a more chaotic sill architecture where many fractures develop above the sills, and are abandoned after a short distance. However, this is limited to the orientation of the outcrop, as we are currently observing the emplacement of the sill parallel to propagation.

Discoloration, or bleaching, has commonly been observed close to sills in the Cedar Mountains (e.g. Figures 3, 5, 6, 7d). At first glance, these bleached zones could provide great analogues for contact metamorphism zones caused by sills, which are found in

the Vøring and Møre basins (e.g. Aarnes et al., 2015). However, the bleached host rocks around the sills in Cedar Mountains appear to be influenced by hydrothermal fluids and not necessarily by the thickness of the intrusions, which is evident by more prominent bleaching within massive sandstone compared to mudstone units. Also, thick sandstone beds around the sills typically show thick bleached zones, which appear to stop at the margins of low-permeability beds, and low-permeability rocks show narrow bleached zones (e.g. Figure 7b). This coincides with recent studies by Skurtveit et al. (2021), which suggest that similar bleaching of the Entrada sandstones is associated with high porosity and high permeability layers, implying a sedimentary facies control on the potential for pervasive bleaching along such layers. Furthermore, bleaching of the Entrada Formation has been found to reduce fracture toughness by 40%, through dissolution of haematite grains and carbonate cement (Major et al., 2018; Skurtveit et al., 2021). This has also been demonstrated by Espinoza et al. (2018), which found a reduction in shear strength and stiffness in altered samples from bleached Entrada sandstones due to CO_2 fluid alteration. However, these studies were focused on migration of CO_2-, CH_4-rich groundwaters and H_2S in potential reservoirs. The sandstones in Cedar Mountains are bleached close to alkaline magma, and such magmas are generally associated with CO_2 and CH_4 degassing (e.g. Konnerup-Madsen et al., 1981). It is therefore a possibility that the bleaching of the host rocks might have a secondary effect on sill emplacement, due to the reduction of fracture toughness of the host rock, originating potentially in the tip cavity in front of the sills. However, this subject is still very limited and the timing and effects of bleaching on petrophysical and geomechanical properties are poorly understood. There are no observations suggesting that the bleaching of the host rocks occurred faster than the propagation of magma.

Sills emplaced within massive sandstone and sandstone units within the heteroliths do not exhibit the same blunt tips as they do within the mudstone layers (e.g. Figure 7b,e). They are sharp and resemble the tips traditionally associated with the tensile fracture-splitting model (e.g. Kavanagh et al., 2013; Pollard & Segall, 1987). The sills in massive sandstone show elastic bending of the host rocks above the intrusion (e.g. Figure 5d), similar to the splays in mudstones. The proposed mechanism for sills in massive sandstone and their respective geometry is that the sills emplace in this lithology mainly while transgressing through the basin. Sills are preferentially emplaced within weaker rocks, such as mudstones and heteroliths. Most sills in the massive sandstone transgress from the base to the top of this layer, as the contact

is seldom parallel. Multiple splays also suggest that there is no strong lithological contact to exploit in this layer and that it is favourable and more energy efficient for the intrusions to transgress through massive sandstones rather than propagating within them.

6.1.3 | Sill emplacement and geometry in heteroliths

Almost half of the sills base contact in the Cedar Mountains are found within heterolithic intervals (52%), which make up 39% of the sedimentary outcrop. This infers a relative probability of 75% of having sill intrusions within heterolithic intervals. The heteroliths feature variable sill geometries, since this lithology includes both mudstone and massive sandstone. The interbedding of mudstone and sandstone occurs at different scales, as the thickness of each lithological unit may vary from a couple of centimetres to meters in thickness. Heteroliths provide therefore a complex heterogeneous lithology filled with weak contacts between layers, mudstones, and anhydrites for the sill to exploit during emplacement (e.g. Figure 5b). Thus, the sills may follow selected horizons within the heteroliths for large distances, while also showing multiple minor broken bridges. This is evident by the stepping and undulating nature of sills within this lithology (Figure 6a). About 80% of all broken- and unbroken bridges with a vertical jog of less than 10 m are found within the heteroliths. The heteroliths commonly exhibit anhydrite veins as well, which appear to be highly favourable for the sills (Figure 5b) due to their weak nature and low fracture toughness.

The sills within the heterolithic intervals generally show blunted tips in mudstone units, similar to Figure 5d but may also feature sharper tips close to bridges and within more sandy layers (Figure 7c). In addition, multiple weak layer contacts are exploited by the sill to promote brittle emplacement structures such as steps and bridges. The vertical jumps of sill splays are different from the one observed in the massive sandstones, as these may also follow their respective layers for a few centimetres to meters before they coalescence with overlaying splays (Figure 7a).

6.2 | Implications for imaging and interpretation of subsurface sills

The Northeastern section of Cedar Mountain sills provides a world-class dataset of sills with variable morphologies that propagate through heterogeneous sedimentary units. Consequently, an outcrop with such detail provides an excellent opportunity to elucidate how the change in morphology would be imaged in a reflection seismic dataset by using the geometry of this sill as input to synthetic seismic modelling, as we have shown in Figure 8. The investigated sill also shows a clear change in morphology based on the host rock it propagates within, as it is generally layer-parallel in mudstones, alternates between horizons on a tens-of-meters-scale in heterolithic rocks and is overall transgressive in sandstones. This raises the interesting possibility of whether it is possible to investigate host-rock properties in subsurface seismic datasets by using the geometry of igneous sill as a proxy for host rock.

Previous work on intrusions has shown that emplacement may change based on host rock properties such as lithology (e.g. mudstones or massive sandstones) consolidation (well or poorly consolidated), and cohesion (e.g. porosity and permeability) (e.g. Schofield, Brown, et al., 2012). In principle, igneous intrusions are well-imaged in seismic datasets due to the high density and velocity contrast between mafic intrusions and sedimentary host rocks (Eide et al., 2018; Smallwood & Maresh, 2002). The geometry and emplacement of the sills highlight the complexity that occurs on a smaller scale with large sheet intrusions: (i) multiple splays, (ii) steps and bridges and (iii) alteration and fracturing of host rocks. These structures often fall beneath seismic resolution due to their small vertical scale but may prove to have an influence on sill geometry. This study has shown that we can expect different emplacement behaviour in different lithologies, such as strata-discordant sills through thicker sandstone layers (e.g. Figures 6 and 7) or multiple strata-concordant intrusions in heterolithic intervals (e.g. Figures 5a,b and 6). Such sill geometries have a strong link to their respective host rocks and can be distinguishable in seismic datasets on shallow depths, where it is possible to distinguish between strata-concordant and discordant sills and in some cases sill segmentation (through broken and unbroken bridges). In deeper datasets (>3 km), however, these sill attributes may either be hidden or interpreted as noise due to low resolution or overprint by multiple reflections.

Seismic modelling based on field analogues is a useful way to assess the validity of seismic interpretation and to study true geometries that can be expected in the subsurface (e.g. Eide et al., 2018; Magee et al., 2014; Rabbel et al., 2018). The synthetic seismic models created in this study show that all three sill segments are imaged with different seismic resolution (Figure 8), but overlapping and underlapping sill segments (e.g. Schofield, Heaton, et al., 2012; Figure 5c), in addition to details and features occurring between sill segments (e.g. unbroken bridges, splays, fractures), often fall beneath seismic resolution. Higher resolution often provides more detail which makes it possible to distinguish over- and underlapping sill segment geometries to distinguish if a bridge is broken or

unbroken. This is shown in Figure 8, where the unbroken bridge between major sill Segment B and C appears as a continuous reflector in 20 Hz resolution but is properly imaged as two separate reflectors in 30 Hz resolution. This observation is also consistent with the increasing number of broken bridges distinguishable within major sill Segment C with increasingly higher resolution. The major difference here is observed between the maximum dip of 30°–45°. Maximum imageable dip is associated with seismic quality and lateral resolution and has been found to rapidly decrease with depth and complexity of overburden (Eide et al., 2018). For instance, only rays with steep incidence angles may reach the target in models with high-velocity layers (i.e. complex overburden), as lower incidence angle rays are refracted away from the target (Eide et al., 2018, 2022; Figure 7b). None of the synthetic seismic models show isolated splays beneath the lower margin of the sill.

This study suggests that mapped sill geometries in seismic datasets can be used to correlate host rocks from available well data. Linking sedimentary strata from well logs to sill geometry could be used to understand sill emplacement mechanisms and propagation of igneous intrusions. However, it is important to emphasize that seismic expression on sill geometry needs to be explicitly viewed from the perspective of their respective sedimentary basin. General statements based on specific geometrical attributes of sills should be avoided to a certain extent, as this could provide potential pitfalls for seismic interpretations.

7 | CONCLUSIONS

This study has presented a field example of a seismic scale mafic sill complex in sedimentary basins. Both host rocks and the igneous intrusions have been described in detail with the help of high-resolution (1.12–3.96 cm/pixel) three-dimensional photogrammetric models, in addition to field observations of the sills and sedimentary host rocks in Utah, US. These models have further been used to develop synthetic seismic modes. The high quality and large extent of the exposures and the high resolution of investigation have allowed the emplacement relationships of the sills down to the centimetre scale to be investigated, especially in terms of host-rock control on sill morphology. Furthermore, a seismic modelling study has been conducted to investigate if and under which circumstances, it is possible to use features on sill margins to constrain subsurface lithology in undrilled basins. The findings of this study are as follows:

- Lithological intervals have a critical control on the style of emplacement of sheet intrusions, shown by the extent of sills within certain levels of the stratigraphy and by the detailed lithological relationships within certain sedimentary packages.
- Sills emplaced within massive sandstone appear most often discordant to strata, heterolithic intervals contain multiple smaller sills that connect through broken bridges, while mudstone features strong strata-concordant sill geometry.
- It is more likely that sills will intrude along discontinuities either consisting of- or including mudstone. In the Cedar Mountain dataset, sills are 3.7 times more likely to emplace within mudstone than in sandstone and/or heterolithic intervals.
- Synthetic seismic models were made to investigate how sills such as the Cedar Mountain sill would appear in standard-quality reflection seismic data at depths of ca. 3 km, showing that vertical jogs and marginal sill features are seldom imaged. For instance, broken- and unbroken bridges (overlapping segments) are difficult to imagine in seismic data, especially splays (i.e. magma-filled fractures) that occur within unbroken bridges.
- Maximum imageable dip of strata is a key factor in detecting sill marginal features (complexity) and smaller scale segmentation. For instance, most bridges with a vertical jog of less than 10 m, and sill splays, occur within heterolithic intervals and often fall beneath the seismic resolution. They are generally more detectable with higher maximum imageable dip.
- Geometries observed in the synthetic seismic models are consistent within the field-based three-dimensional model, which may provide knowledge on how to interpret sills in seismic datasets with existing well logs to predict host rock lithology.
- Strata-discordant sills often suggest massive sandstone layers with little to no discontinuities or sedimentary structures. Strata-concordant sills, often with detectable vertical jogs, suggest heterolithic intervals or mudstone.

In sum, this implies that lithology has a strong control on the geometry and morphology of sills, which can even be detected in high-quality seismic datasets. It is crucial to understand the segmentation and geometry of sills to predict stratigraphy and sedimentology of the host rocks, as the sills expression is a direct response to the state of the host rocks.

CONFLICT OF INTEREST STATEMENT

The authors declare that they have no known competing financial interests or personal relationships that could have appeared to influence the work reported in this paper.

PEER REVIEW

The peer review history for this article is available at https://www.webofscience.com/api/gateway/wos/peer-review/10.1111/bre.12857.

DATA AVAILABILITY STATEMENT

The data that support the findings of this study are available from the corresponding author upon reasonable request. The three-dimensional models will be uploaded to v3geo in the near future.

ORCID

Martin Kjenes https://orcid.org/0000-0001-7728-4265
Christian Haug Eide https://orcid.org/0000-0003-4949-9917
Agustin Argüello Scotti https://orcid.org/0000-0002-4547-183X
Isabelle Lecomte https://orcid.org/0000-0002-3316-535X
Nick Schofield https://orcid.org/0000-0002-3083-735X

REFERENCES

Aarnes, I., Planke, S., Trulsvik, M., & Svensen, H. (2015). Contact metamorphism and thermogenic gas generation in the Vøring and Møre basins, offshore Norway, during the Paleocene–Eocene thermal maximum. *Journal of the Geological Society*, *172*(5), 588–598.

Abdelmalak, M. M., Mourgues, R., Galland, O., & Bureau, D. (2012). Fracture mode analysis and related surface deformation during dyke intrusion: Results from 2D experimental modelling. *Earth and Planetary Science Letters*, *359*, 93–105.

Airoldi, G., Muirhead, J. D., White, J. D., & Rowland, J. (2011). Emplacement of magma at shallow depth: Insights from field relationships at Allan Hills, south Victoria Land, East Antarctica. *Antarctic Science*, *23*(3), 281–296.

Anderson, O. J., & Lucas, S. G. (1994). Middle Jurassic stratigraphy, sedimentation and paleogeography in the southern Colorado Plateau and southern High Plains. *Rocky Mountain Section (SEPM)*, 299–314.

Bjerrum, C. J., & Dorsey, R. J. (1995). Tectonic controls on deposition of Middle Jurassic strata in a retroarc foreland basin, Utah-Idaho trough, western interior, United States. *Tectonics*, *14*(4), 962–978.

Bunger, A. P., & Cruden, A. R. (2011). Modeling the growth of laccoliths and large mafic sills: Role of magma body forces. *Journal of Geophysical Research: Solid Earth*, *116*(B2), 1–18.

Burchardt, S., Mattsson, T., Palma, J. O., Galland, O., Almqvist, B., Mair, K., Jerram, D. A., Hammer, Ø., & Sun, Y. (2019). Progressive growth of the Cerro Bayo cryptodome, Chachahuén volcano, Argentina—Implications for viscous magma emplacement. *Journal of Geophysical Research: Solid Earth*, *124*(8), 7934–7961.

Cartwright, J., & Møller Hansen, D. (2006). Magma transport through the crust via interconnected sill complexes. *Geology*, *34*(11), 929–932.

Collinson, J. (2019). *Sedimentary structures*. Dunedin Academic Press Ltd.

Crabaugh, M., & Kocurek, G. (1993). Entrada sandstone: An example of a wet aeolian system. *Geological Society, London, Special Publications*, *72*(1), 103–126.

Delaney, P. T., & Gartner, A. E. (1997). Physical processes of shallow mafic dike emplacement near the San Rafael Swell, Utah. *Geological Society of America Bulletin*, *109*(9), 1177–1192.

Díez, M., Connor, C. B., Kruse, S. E., Connor, L., & Savov, I. P. (2009). Evidence of small-volume igneous diapirism in the shallow crust of the Colorado Plateau, San Rafael Desert, Utah. *Lithosphere*, *1*(6), 328–336.

Doelling, H. H., Kuehne, P. A., Willis, G. C., & Ehler, J. B. (2015). *Geologic map of the San Rafael Desert 30′ × 60′ quadrangle, Emery and Grand Counties, Utah*. Utah Geological Survey, Map 267DM, scale 1:62,500.

Donnadieu, F., & Merle, O. (1998). Experiments on the indentation process during cryptodome intrusions: New insights into Mount St. Helens deformation. *Geology*, *26*(1), 79–82.

Duffield, W. A., Bacon, C. R., & Delaney, P. T. (1986). Deformation of poorly consolidated sediment during shallow emplacement of a basalt sill, Coso Range, California. *Bulletin of Volcanology*, *48*, 97–107.

Eide, C. H., Schofield, N., Howell, J., & Jerram, D. A. (2022). Transport of mafic magma through the crust and sedimentary basins: Jameson Land, East Greenland. *Journal of the Geological Society*, *179*(3), jgs2021-043.

Eide, C. H., Schofield, N., Jerram, D. A., & Howell, J. A. (2017). Basin-scale architecture of deeply emplaced sill complexes: Jameson Land, East Greenland. *Journal of the Geological Society*, *174*(1), 23–40.

Eide, C. H., Schofield, N., Lecomte, I., Buckley, S. J., & Howell, J. A. (2018). Seismic interpretation of sill complexes in sedimentary basins: Implications for the sub-sill imaging problem. *Journal of the Geological Society*, *175*(2), 193–209.

Espinoza, D. N., Jung, H., Major, J. R., Sun, Z., Ramos, M. J., Eichhubl, P., Balhoff, M. T., Choens, R. C., & Dewers, T. A. (2018). CO_2 charged brines changed rock strength and stiffness at Crystal Geyser, Utah: Implications for leaking subsurface CO_2 storage reservoirs. *International Journal of Greenhouse Gas Control*, *73*, 16–28.

Flecha, I., Carbonell, R., Hobbs, R. W., & Zeyen, H. (2011). Some improvements in subbasalt imaging using pre-stack depth migration. *Solid Earth*, *2*(1), 1–7.

Fliedner, M. M., & White, R. S. (2003). Depth imaging of basalt flows in the Faeroe-Shetland Basin. *Geophysical Journal International*, *152*(2), 353–371.

Gallagher, J. W., & Dromgoole, P. W. (2007). Exploring below the basalt, offshore Faroes: A case history of sub-basalt imaging. *Petroleum Geoscience*, *13*(3), 213–225.

Galland, O., Spacapan, J. B., Rabbel, O., Mair, K., Soto, F. G., Eiken, T., & Leanza, H. A. (2019). Structure, emplacement mechanism and magma-flow significance of igneous fingers–Implications for sill emplacement in sedimentary basins. *Journal of Structural Geology*, *124*, 120–135.

Germa, A., Koebli, D., Wetmore, P., Atlas, Z., Arias, A., Savov, I. P., Diez, M., Greaves, V., & Gallant, E. (2020). Crystallization and segregation of syenite in shallow mafic sills: Insights from the San Rafael Subvolcanic field, Utah. *Journal of Petrology*, *61*(9), egaa092.

Gill, S. P. A., & Walker, R. J. (2020). The roles of elastic properties, magmatic pressure, and tectonic stress in saucer-shaped sill growth. *Journal of Geophysical Research: Solid Earth*, *125*(4), e2019JB019041.

Gilluly, J. (1927). Analcite diabase and related alkaline syenite from Utah. *American Journal of Science*, *5*(81), 199–211.

Gilmullina, A., Klausen, T. G., Paterson, N. W., Suslova, A., & Eide, C. H. (2021). Regional correlation and seismic stratigraphy of Triassic Strata in the Greater Barents Sea: Implications for sediment transport in Arctic basins. *Basin Research*, *33*(2), 1546–1579.

Gonzales, D. A., & Lake, E. T. (2017). Geochemical constraints on mantle-melt sources for Oligocene to Pleistocene mafic rocks in the Four Corners region, USA. *Geosphere*, *13*(1), 201–226.

Gross, E. C., Carr, M., & Jobe, Z. R. (2023). Three-dimensional bounding surface architecture and lateral facies heterogeneity of a wet aeolian system: Entrada Sandstone, Utah. *Sedimentology*, *70*(1), 145–178.

Haug, Ø. T., Galland, O., Souloumiac, P., Souche, A., Guldstrand, F., & Schmiedel, T. (2017). Inelastic damage as a mechanical precursor for the emplacement of saucer-shaped intrusions. *Geology*, *45*(12), 1099–1102.

Haug, Ø. T., Galland, O., Souloumiac, P., Souche, A., Guldstrand, F., Schmiedel, T., & Maillot, B. (2018). Shear versus tensile failure mechanisms induced by sill intrusions: Implications for emplacement of conical and saucer-shaped intrusions. *Journal of Geophysical Research: Solid Earth*, *123*(5), 3430–3449.

Holford, S., Schofield, N., MacDonald, J., Duddy, I., & Green, P. (2012). Seismic analysis of igneous systems in sedimentary basins and their impacts on hydrocarbon prospectivity: Examples from the southern Australian margin. *The APPEA Journal*, *52*(1), 229–252.

Humphreys, E. D. (1995). Post-Laramide removal of the Farallon slab, western United States. *Geology*, *23*(11), 987–990.

Jerram, D. A., & Bryan, S. E. (2018). Plumbing systems of shallow level intrusive complexes. In C. Breitkreuz & S. Rocchi (Eds.), *Physical Geology of Shallow Magmatic Systems* (pp. 39–60). Springer.

Kallweit, R. S., & Wood, L. C. (1982). The limits of resolution of zero-phase wavelets. *Geophysics*, *47*, 1035–1046.

Kavanagh, J. L., Menand, T., & Daniels, K. A. (2013). Gelatine as a crustal analogue: Determining elastic properties for modelling magmatic intrusions. *Tectonophysics*, *582*, 101–111.

Kavanagh, J. L., Menand, T., & Sparks, R. S. J. (2006). An experimental investigation of sill formation and propagation in layered elastic media. *Earth and Planetary Science Letters*, *245*(3–4), 799–813.

Kavanagh, J. L., Rogers, B. D., Boutelier, D., & Cruden, A. R. (2017). Controls on sill and dyke-sill hybrid geometry and propagation in the crust: The role of fracture toughness. *Tectonophysics*, *698*, 109–120.

Kiyosugi, K., Connor, C. B., Wetmore, P. H., Ferwerda, B. P., Germa, A. M., Connor, L. J., & Hintz, A. R. (2012). Relationship between dike and volcanic conduit distribution in a highly eroded monogenetic volcanic field: San Rafael, Utah, USA. *Geology*, *40*(8), 695–698.

Kjenes, M., Eide, C. H., Schofield, N., & Chedburn, L. (2023). Alkaline sill intrusions in sedimentary basins: Emplacement of the Mussentuchit Wash Sill in San Rafael Swell, Utah. *Journal of the Geological Society*, *180*(1), jgs2021-139.

Kocurek, G. (1981). Significance of interdune deposits and bounding surfaces in aeolian dune sands. *Sedimentology*, *28*(6), 753–780.

Kocurek, G., & Havholm, K. G. (1993). Eolian sequence stratigraphy—A conceptual framework: Chapter 16: Recent developments in siliciclastic sequence stratigraphy.

Kokelaar, B. P. (1982). Fluidization of wet sediments during the emplacement and cooling of various igneous bodies. *Journal of the Geological Society*, *139*(1), 21–33.

Konnerup-Madsen, J., Rose-Hansen, J., & Larsen, E. (1981). Hydrocarbon gases associated with alkaline igneous activity: Evidence from compositions of fluid inclusions. *Rapport Grønlands Geologiske Undersøgelse*, *103*, 99–108.

Lecomte, I., Lavadera, P. L., Anell, I., Buckley, S. J., Schmid, D. W., & Heeremans, M. (2015). Ray-based seismic modeling of geologic models: Understanding and analyzing seismic images efficiently. *Interpretation*, *3*, SAC71–SAC89.

Lecomte, I., Lavadera, P. L., Botter, C., Anell, I., Buckley, S. J., Eide, C. H., Grippa, A., Mascolo, V., & Kjoberg, S. (2016). 2 (3) D convolution modelling of complex geological targets beyond—1D convolution. *First Break*, *34*(5), 99–107.

Luedke, R. G., & Smith, R. L. (1984). Map showing distribution, composition, and age of late Cenozoic volcanic centers in the western conterminous United States (No. 1523).

Magee, C., Jackson, C. L., & Schofield, N. (2014). Diachronous sub-volcanic intrusion along deep-water margins: Insights from the Irish Rockall Basin. *Basin Research*, *26*(1), 85–105.

Magee, C., Muirhead, J. D., Karvelas, A., Holford, S. P., Jackson, C. A., Bastow, I. D., Schofield, N., Stevenson, C. T., McLean, C., McCarthy, W., & Shtukert, O. (2016). Lateral magma flow in mafic sill complexes. *Geosphere*, *12*(3), 809–841.

Magee, C., Stevenson, C., O'driscoll, B., Schofield, N., & McDermott, K. (2012). An alternative emplacement model for the classic Ardnamurchan cone sheet swarm, NW Scotland, involving lateral magma supply via regional dykes. *Journal of Structural Geology*, *43*, 73–91.

Major, J. R., Eichhubl, P., Dewers, T. A., & Olson, J. E. (2018). Effect of CO_2–brine–rock interaction on fracture mechanical properties of CO_2 reservoirs and seals. *Earth and Planetary Science Letters*, *499*, 37–47.

Mathieu, L., de Vries, B. V. W., Holohan, E. P., & Troll, V. R. (2008). Dykes, cups, saucers and sills: Analogue experiments on magma intrusion into brittle rocks. *Earth and Planetary Science Letters*, *271*(1–4), 1–13.

Michaut, C. (2011). Dynamics of magmatic intrusions in the upper crust: Theory and applications to laccoliths on Earth and the Moon. *Journal of Geophysical Research: Solid Earth*, *116*(B5), B05205.

Mitten, A. J., Howell, L. P., Clarke, S. M., & Pringle, J. K. (2020). Controls on the deposition and preservation of architectural elements within a fluvial multi-storey sandbody. *Sedimentary Geology*, *401*, 105629.

Mudge, M. R. (1968). Depth control of some concordant intrusions. *Geological Society of America Bulletin*, *79*(3), 315–332.

Pederson, J. L., Mackley, R. D., & Eddleman, J. L. (2002). Colorado Plateau uplift and erosion evaluated using GIS. *GSA Today*, *12*(8), 4–10.

Peterson, F. (1988). Pennsylvanian to Jurassic eolian transportation systems in the western United States. *Sedimentary Geology*, *56*(1–4), 207–260.

Planke, S., Svensen, H., Myklebust, R., Bannister, S., Manton, B., & Lorenz, L. (2018). Geophysics and remote sensing. In C. Breitkreuz & S. Rocchi (Eds.), *Physical geology of shallow magmatic systems: Dykes, sills, and laccoliths* (pp. 131–146). Springer.

Pollard, D. D. (1973). Derivation and evaluation of a mechanical model for sheet intrusions. *Tectonophysics*, *19*(3), 233–269.

Pollard, D. D., & Segall, P. (1987). Theoretical displacements and stresses near fractures in rock: With application to faults, joints, veins, dikes and solution surfaces. In B. Atkinson (Ed.), *Fracture mechanics of rock*. London: Academic Press. https://doi.org/10.1016/C2009-0-21691-6

Rabbel, O., Galland, O., Mair, K., Lecomte, I., Senger, K., Spacapan, J. B., & Manceda, R. (2018). From field analogues to realistic seismic modelling: A case study of an oil-producing andesitic sill complex in the Neuquén Basin, Argentina. *Journal of the Geological Society*, *175*(4), 580–593.

Reid, M. R., Bouchet, R. A., Blichert-Toft, J., Levander, A., Liu, K., Miller, M. S., & Ramos, F. C. (2012). Melting under the Colorado Plateau, USA. *Geology*, *40*(5), 387–390.

Richardson, J. A., Connor, C. B., Wetmore, P. H., Connor, L. J., & Gallant, E. A. (2015). Role of sills in the development of volcanic fields: Insights from lidar mapping surveys of the San Rafael Swell, Utah. *Geology*, *43*(11), 1023–1026.

Rohrman, M. (2013). Intrusive large igneous provinces below sedimentary basins: An example from the Exmouth Plateau (NW Australia). *Journal of Geophysical Research: Solid Earth*, *118*(8), 4477–4487.

Rubin, A. M. (1993). Tensile fracture of rock at high confining pressure: Implications for dike propagation. *Journal of Geophysical Research: Solid Earth*, *98*(B9), 15919–15935.

Schmiedel, T., Galland, O., & Breitkreuz, C. (2017). Dynamics of sill and laccolith emplacement in the brittle crust: Role of host rock strength and deformation mode. *Journal of Geophysical Research: Solid Earth*, *122*(11), 8860–8871.

Schofield, N., Heaton, L., Holford, S. P., Archer, S. G., Jackson, C. A. L., & Jolley, D. W. (2012). Seismic imaging of 'broken bridges': Linking seismic to outcrop-scale investigations of intrusive magma lobes. *Journal of the Geological Society*, *169*(4), 421–426.

Schofield, N., Stevenson, C., & Reston, T. (2010). Magma fingers and host rock fluidization in the emplacement of sills. *Geology*, *38*(1), 63–66.

Schofield, N. J., Brown, D. J., Magee, C., & Stevenson, C. T. (2012). Sill morphology and comparison of brittle and non-brittle emplacement mechanisms. *Journal of the Geological Society*, *169*(2), 127–141.

Senger, K., Millett, J., Planke, S., Ogata, K., Eide, C. H., Festøy, M., & Jerram, D. A. (2017). Effects of igneous intrusions on the petroleum system: a review. *First Break*, *35*, 47–56.

Skilling, I. P., White, J. D., & McPhie, J. (2002). Peperite: A review of magma–sediment mingling. *Journal of Volcanology and Geothermal Research*, *114*(1–2), 1–17.

Skurtveit, E., Torabi, A., Sundal, A., & Braathen, A. (2021). The role of mechanical stratigraphy on CO_2 migration along faults–examples from Entrada Sandstone, Humbug Flats, Utah, USA. *International Journal of Greenhouse Gas Control*, *109*, 103376.

Smallwood, J. R., & Maresh, J. (2002). The properties, morphology, and distribution of igneous sills: Modelling, borehole data and 3D seismic. *The North Atlantic Igneous Province: Stratigraphy, Tectonic, Volcanic, and Magmatic Processes*, *197*, 271.

Spacapan, J. B., Galland, O., Leanza, H. A., & Planke, S. (2017). Igneous sill and finger emplacement mechanism in shale-dominated formations: A field study at Cuesta del Chihuido, Neuquén Basin, Argentina. *Journal of the Geological Society*, *174*(3), 422–433.

Stephens, T. L., Walker, R. J., Healy, D., & Bubeck, A. (2021). Segment tip geometry of sheet intrusions, II: Field observations of tip geometries and a model for evolving emplacement mechanisms. *Volcanica*, *4*(2), 203–225.

Thompson, G. A., & Zoback, M. L. (1979). Regional geophysics of the Colorado Plateau. *Tectonophysics*, *61*(1–3), 149–181.

Thomson, K., & Hutton, D. (2004). Geometry and growth of sill complexes: Insights using 3D seismic from the North Rockall Trough. *Bulletin of Volcanology*, *66*, 364–375.

Tingey, D. G., Christiansen, E. H., Best, M. G., Ruiz, J., & Lux, D. R. (1991). Tertiary minette and melanephelinite dikes, Wasatch Plateau, Utah: Records of mantle heterogeneities and changing tectonics. *Journal of Geophysical Research: Solid Earth*, *96*(B8), 13529–13544.

Yao, Z., & Mungall, J. E. (2022). Transport and deposition of immiscible sulfide liquid during lateral magma flow. *Earth-Science Reviews*, *227*, 103964.

Zhai, M., Wang, D., Wang, L., Wang, K., Shi, H., Xiao, F., & Li, L. (2021). Numerical simulation and optimization of hydraulic fracturing operation in a sandstone-mudstone interbedded reservoir. *Arabian Journal of Geosciences*, *14*, 1–22.

Zuchuat, V., Sleveland, A., Sprinkel, D., Rimkus, A., Braathen, A., & Midtkandal, I. (2018). New insights on the impact of tidal currents on a low-gradient, semi-enclosed, epicontinental basin—The Curtis Formation, east-central Utah, USA. *Geology of the Intermountain West*, *5*, 131–165.

Zuchuat, V., Sleveland, A. R., Pettigrew, R. P., Dodd, T. J., Clarke, S. M., Rabbel, O., Braathen, A., & Midtkandal, I. (2019). Overprinted allocyclic processes by tidal resonance in an epicontinental basin: The upper Jurassic Curtis formation, east-central Utah, USA. *The Depositional Record*, *5*(2), 272–305.